Temperature and time-controlled etching of carbon fiber nanotip electrodes: Creating nanocavity- and nanodot-modified surfaces for

Carbon 243 (2025) 120612

Contents lists available at ScienceDirect

Carbon

journal homepage: www.elsevier.com/locate/carbon

Temperature and time-controlled etching of carbon fiber nanotip electrodes: Creating nanocavity- and nanodot-modified surfaces for enhanced neurotransmitter detection

Pankaj Gupta [a], Ajay Pradhan [b], Vandna K. Gupta [a], Hanna Karlsson-Fernberg [a], Yuanmo Wang [a], Jörg Hanrieder [b,c,d,e], Henrik Zetterberg [b,c,d,e,f,g], Ann-Sofie Cans [a,*]

[a] Department of Chemistry and Chemical Engineering, Chalmers University of Technology, Kemigården 4, Gothenburg, 412 96, Sweden
[b] Department of Psychiatry and Neurochemistry, Institute of Neuroscience & Physiology, The Sahlgrenska Academy at the University of Gothenburg, Mölndal, 431 80, Sweden
[c] Clinical Neurochemistry Laboratory, Sahlgrenska University Hospital, Mölndal, 431 80, Sweden
[d] Department of Neurodegenerative Disease, UCL Institute of Neurology, Queen Square, London, WC1N 3BG, UK
[e] UK Dementia Research Institute at UCL, London, WC1N 3BG, UK
[f] Hong Kong Center for Neurodegenerative Diseases, Clear Water Bay, 999077, Hong Kong, China
[g] Wisconsin Alzheimer's Disease Research Center, University of Wisconsin School of Medicine and Public Health, University of Wisconsin-Madison, Madison, WI, 53726, USA

ARTICLE INFO

Keywords:
Carbon fiber nanotip electrode
Nanostructured surface
Heat etching
SH-SY5Y cells
Neurotransmitters
Amperometry

ABSTRACT

Carbon fiber has become the standard electrode material to study neuronal communication. For techniques such as single-cell amperometry at synapses and intracellular recordings of neurotransmitters in secretory vesicles, nanometric electrodes are required. The smaller electrode dimension also offers the added benefit of low background noise during amperometric recordings. To fabricate nanotip electrodes with suitable size and geometry, the carbon fiber is generally etched using flame- or electrochemical etching. However, current methods suffer from low reproducibility and poor success rates. In this work, we present a novel, simple-to-use method for fabricating highly sensitive pointy electrodes with tip diameters of ~150 nm. This method uses the controlled heat from a time- and temperature-regulated metal heating filament of a micropipette puller. Scanning electron microscopy showed that electrodes produced by this approach exhibit a rough surface densely covered with carbon nanocavities and nanodots, forming an intricate and unique surface structure. Further, characterization using energy dispersive spectroscopy, Raman microscopy, square wave and cyclic voltammetry revealed an increased abundance of graphitic edge plane defects at the electrode surface, resulting in a remarkable increase in sensitivity and electron transfer kinetics for the detection of redox-analytes and multiple catecholamine neurotransmitters while reducing surface fouling. Limiting the nanoelectrode tip length to ~10 μm and inserting it into the cytoplasm of SH-SY5Y cells resulted in excellent low-noise amperometric recordings of intracellular norepinephrine content stored in individual secretory vesicles, which serves as a great proof of concept for the use of these nanostructured electrodes for studies on neurotransmission at single cells.

1. Introduction

Carbon fiber electrodes have been predominantly used in the past decades for qualitative and quantitative studies of neurotransmitter release from both neuronal and non-neuronal cells using electrochemical amperometry and voltammetric techniques [1–5]. Properties such as high electrical conductivity, wide operating potential window, chemical inertness, biocompatibility, and resistance to biofouling make carbon fiber an attractive electrode material for studying neurotransmission at single cells and for *in vivo* brain recordings [4,6,7]. By placing a carbon fiber microelectrode in close contact with a secretory cell and simultaneously applying a constant positive potential to the electrode

* Corresponding author.
E-mail address: cans@chalmers.se (A.-S. Cans).

https://doi.org/10.1016/j.carbon.2025.120612
Received 14 April 2025; Received in revised form 10 July 2025; Accepted 12 July 2025
Available online 14 July 2025

sufficiently high enough to drive a oxidation reactions, stimulation-evoked vesicular secretion of neurotransmitters can be recorded with high temporal resolution using amperometry.

Conventional carbon fibers typically range in size from 5 to 30 μm in diameter and are widely used for fabricating glass-insulated disk microelectrodes. While this electrode size range is suitable for fabricating disk-shaped microelectrodes for placement at the soma of single non-neuronal cells [8], cylindrical microelectrodes with protruding, exposed, non-insulated carbon fibers are commonly used for *in vivo* measurements in specific brain regions [5], enabling the study of neurotransmission coupled to behavior and other brain functions. The small dimension of these electrodes makes them suitable for implantation, with minimal tissue damage upon insertion compared to larger probes, like the ones used for microdialysis [9,10]. Since the first use of carbon fiber for catecholamine detection by Ponchon et al. in the early 1980s [11], significant progress has been made in the field, including carbon fiber surface modifications to enhance detection capabilities and reduction in electrode size, with tip diameters reaching nanometric dimensions for intracellular recordings [6,10–12]. As conventional carbon fibers have a smooth surface, past studies have focused on modifying their surface using surface treatment, functionalization, or coatings with carbon nanomaterials to create higher surface roughness [6,13–17]. These surface modifications introduce functional groups or exposure of edge plane graphitic sites that enhance electrode sensitivity, selectivity, and electron transfer kinetics compared to pristine carbon fiber microelectrodes and also confer resistance to fouling by neurochemicals [6, 18–21].

Fabrication of carbon fiber nanotip electrodes (CFNEs) for placement at tiny spaces near neuronal neurites or for insertion into the cell cytoplasm for intracellular recordings is currently limited to a few techniques. The most commonly used techniques in the past decades have been electrochemical etching and flame etching of the exposed carbon fiber at the electrode tip. Electrochemical etching, first performed by Armstrong-James et al. in 1980 to produce pointed carbon fiber tips for brain tissue penetration [22] was later refined by Meulemans et al. [23], Kawagoe et al. [24], Wipf group [25,26] and Roberts et al. [27] to produce submicron sharp carbon fiber electrodes with greater control. However, electrochemical etching typically results in CFNEs with exposed carbon fibers exceeding 100 μm in length. This large electrode surface area results in elevated background noise and a lower signal-to-noise ratio in electrochemical recordings. To minimize noise and enhance sensitivity, excess surface area of the carbon fiber needs to be insulated. This can be solved by electrochemically coating the excess surface with resistive insulating materials, based on phenolic monomers, while masking a desired length of the electrode tip [27]. However, this step is technically challenging, which risks damaging the tip and suffers from poor reproducibility due to the variability in the exposed tip length.

Flame etching, introduced by Strein and Ewing [28], is the second most commonly used CFNE fabrication method, which involves slowly passing the cylindrical carbon fiber microelectrode tip through the core of a butane flame by hand to create nanotip electrodes with a tip diameter of roughly 100 nm. Compared to electrochemical etching, flame-etched CFNEs offer higher sensitivity due to moderate heat-induced nanometric surface modifications [29]. These electrodes have been used for intracellular recordings of neurotransmitter release from secretory vesicles upon contact with the electrode surface [30,31]. However, this fabrication method suffers from a low success rate and poor reproducibility, producing CFNEs with tip lengths varying between 30 and 100 μm [29]. This technique relies on manual manipulation of the electrode tip into the flame while constantly rotating it for about 1–3 s, making precise control over the etching process extremely challenging. Prolonged exposure to the open flame can damage the insulating glass, leading to unstable baselines and increased background noise. Therefore, reliably fabricating CFNEs with precise control over tip dimensions and desired lengths, ideally shorter than 30 μm, remains a significant challenge. An alternative approach using advanced fabrication techniques has been reported by Venton group, offering precise control over the fabrication of nanoelectrodes. However, the fabrication of such electrodes requires sophisticated and expensive instruments not commonly accessible to most research labs [20,32–34]. Strategies for surface functionalization, manipulating the ratio of edge plane versus basal plane sites or the introduction of nanostructures at the carbon surface, have been important for improving the sensitivity, selectivity, and fouling resistance of carbon fiber microelectrodes. However, the current fabrication methods are either struggling with reproducibility, have a low success rate, or have a need for state-of-the-art technologies.

In this study, we introduce a simple-to-use and reliable heat etching method for fabricating highly sensitive CFNEs with nanostructured surfaces and a high fabrication success rate. To produce CFNEs, glass-sealed 5 μm cylindrical carbon fiber microelectrodes with a 200 μm exposed tip were mounted to a micromanipulator and positioned near the heating filament of a glass micropipette puller. By applying a time- and temperature-controlled heating program to the metal filament, the exposed carbon fiber was etched by the applied heat, producing a conical-shaped CFNE with a tip diameter in the hundred nanometer range. The surface chemistry and electrochemical properties of the heat-etched electrodes were characterized and compared to electrodes with similar dimensions prepared using conventional methods, *i.e.*, flame etching and electrochemical etching. Cyclic voltammetry analysis of dopamine, epinephrine, norepinephrine, and serotonin showed that heat-etched electrodes exhibited higher sensitivity and faster electron transfer kinetics than CFNEs fabricated via conventional methods. Surface characterization using field emission scanning electron microscopy (FE-SEM), energy-dispersive X-ray spectroscopy (EDX), and Raman spectroscopy further demonstrated significant differences in surface morphology and modifications to surface chemistry between the CFNEs.

To assess the suitability of heat-etched CFNEs for neurochemical measurements, the electrode lengths were precisely controlled to a range between 8 and 10 μm to minimize the surface area of the non-insulated carbon fiber and reduce background noise during electrochemical recordings. These electrodes were then tested for intracellular amperometric electroanalysis of the secretory vesicle content of the neurotransmitter norepinephrine in SH-SY5Y cells. Upon insertion of the CFNEs into the cell cytoplasm, these electrodes recorded amperometric current trace over time, capturing a multitude of spontaneous sharp current transients, with each spike corresponding to the detection of neurotransmitter release from individual dense core vesicles at the electrode surface. This study presents a new straightforward approach for fabricating nanostructured highly sensitive CFNEs that offer a higher fabrication success rate compared to existing methods. By mounting the electrode in a fixed position relative to the heat source during the etching process, and using pre-programmed temperature and heating time, the method enables precise and reproducible control over electrode length, offering a significant advantage over traditional flame etching, which relies on manual handling and introduces variability. This is particularly beneficial for fabricating shorter, low-noise CFNEs, which are crucial for high-sensitivity vesicular neurotransmitter analysis. Overall, our heat-etching method offers a reliable and reproducible alternative to traditional fabrication methods of CFNEs, providing significant advantages for electrochemical studies of neurotransmission.

2. Materials and methods

2.1. Chemicals and materials

Dopamine, serotonin, epinephrine, norepinephrine and buffer salts were purchased from Sigma-Aldrich. Sodium phosphate buffer of 0.1 M ionic strength and pH of 7.4 was prepared by using Na_2HPO_4 and NaH_2PO_4 as reported by Christian and Purdy [35]. De-identified human CSF samples of three healthy male patients were obtained from Sahlgrenska University Hospital, Göteborg, and used as received without any

purification. The 5 μm in diameter carbon fibers were received from Cytec Engineered Materials, Tempe, USA. For electrochemical characterization of CFNEs, solutions of hexaammineruthenium(III) chloride $[Ru(NH_3)_6]Cl_3$, ferrocene-methanol (FcMeOH), potassium ferricyanide (III) $K_3[Fe(CN)_6]$ and potassium chloride (KCl), (Sigma-Aldrich) were prepared in Milli-Q ultrapure water (18.2 MΩ cm). All other chemical reagents and solvents used in the experiments were of analytical grade and were used as received. Milli-Q water (18 MΩ) was used throughout the experiments.

2.2. Instrumentation

All voltammetric experiments were recorded using a CHI 1030C electrochemical workstation (CH Instruments, Inc. Austin, TX, USA). The experiments were carried out with a single compartment two-electrode mode, equipped with a CFNE as the working electrode and Ag/AgCl (3 M KCl) as the reference electrode (RE) (CH Instruments, Inc. Austin, TX, USA). Surface characterizations were performed using a JEOL JSM-7800F Prime field emission-scanning electron microscopy (FE-SEM) operated at 5 kV acceleration voltage. Raman spectra were collected using an inVia Raman microscope (Renishaw, Gloucestershire, UK), excited by a 532 nm Ar-ion laser. Raman spectra were collected at 5 regions of interest for each electrode sample using ~20 s acquisition time and 1 % power. The reported results represent the average of recorded measurements. The cell measurements were performed using an Axopatch 200B patch clamp amplifier (Molecular Devices, Sunnyvale, CA, USA) equipped with a low-noise digitizer Axon™ Digidata®1550B (Molecular Devices, Sunnyvale, CA, USA).

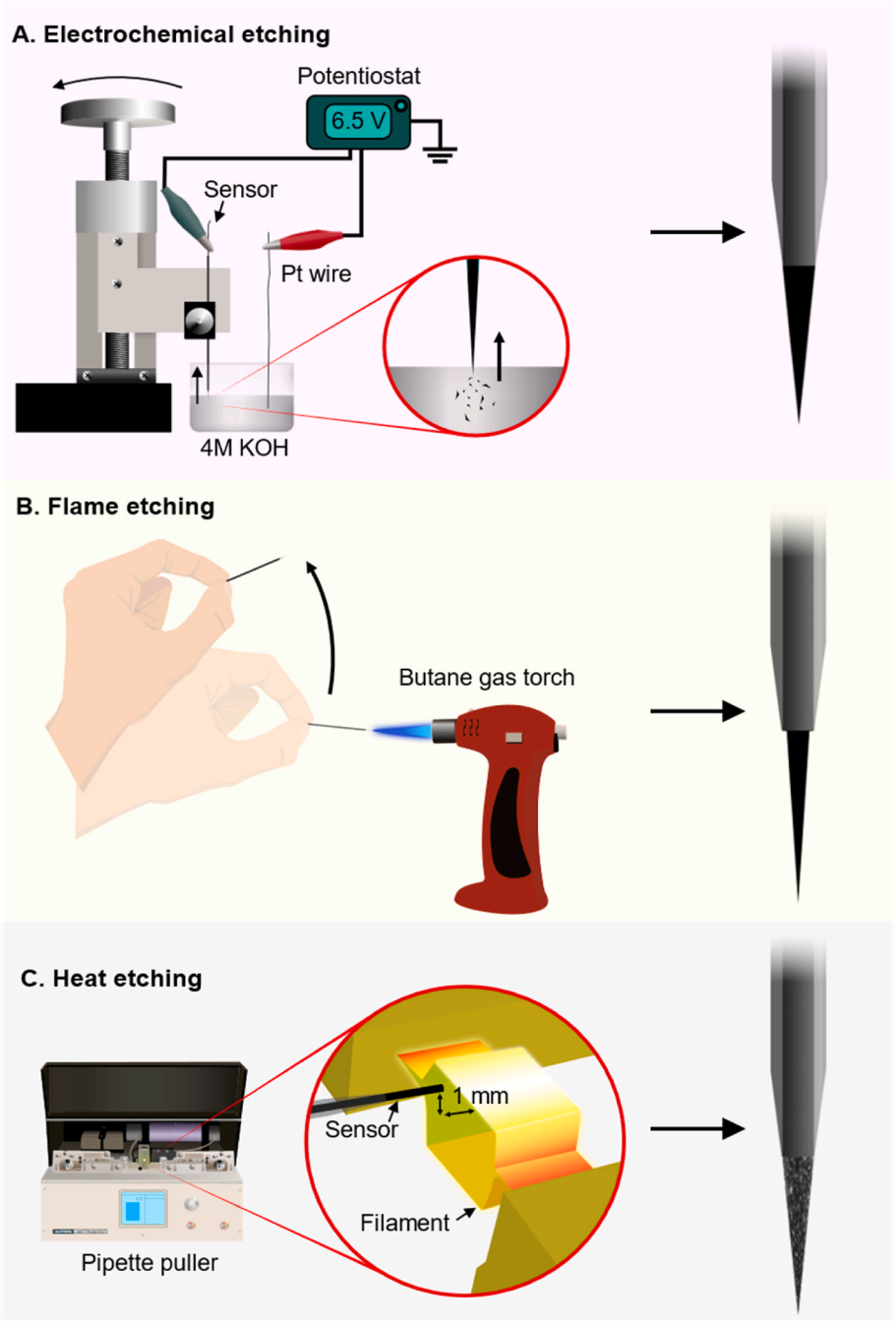

Fig. 1. Schematic for the fabrication of carbon fiber nanotip electrodes (CFNEs) using (A) electrochemical etching, (B) flame-etching and (C) heat-etching.

2.3. Fabrication of electrodes

2.3.1. Fabrication of 5 μm glass insulated cylindrical carbon fiber microelectrodes

Cylindrical carbon fiber microelectrodes were fabricated as previously described [36]. Briefly, single 5 μm in diameter carbon fibers (Cytec Engineered Materials, Tempe, AZ) were aspirated into borosilicate glass capillaries (1 mm OD, 0.5 mm ID, Sutter Instrument Co., Novato, CA). A commercial micropipette puller (P-1000, Sutter Instruments Co., Novato, USA) was used to pull the carbon fiber-filled capillaries to create two tapered glass-coated carbon fiber electrodes. The carbon fibers stretched between the pulled glass tips were disconnected using a scissor and excess carbon fibers extending from the glass seal were cut to a ~200 μm protruding length using a scalpel, under a microscope. The glass-coated carbon fiber tips were then sealed by placing them into epoxy resin (EpoTek 301, Epoxy Technology, Billerica, MA) for 3 min and subsequently dipped into an acetone solution for 15 s to remove the excess epoxy from the electrode tip. Lastly, the epoxy-sealed electrodes were cured in an oven at 100 °C overnight and safely stored until use.

2.3.2. Electrochemical etching of carbon fiber microelectrodes into conical CFNEs

Electrochemically etched CFNEs were prepared according to a previously described method [27]. In brief, the back sides of 5 μm cylindrical carbon fiber microelectrodes were first coupled to a silver metal wire using silver paste to make an electrical connection. The protruding ~200 μm carbon fiber was then electrochemically etched into a cone-shaped nanotip by attaching the electrode to a micromanipulator holder and using it to lower the electrode into a 4 M KOH solution while applying a +6.5 V potential versus a platinum wire for 1–1.5 s (Fig. 1A) and subsequently removing the electrode out of the KOH solution. The fabricated CFNEs were rinsed in distilled water and inspected under a microscope to ensure the successful formation of a nanotip without any damage to the glass.

2.3.3. Flame etching of carbon fiber microelectrodes creates conical CFNEs

Flame-etched CFNEs were prepared according to a previous protocol [31]. Briefly, the protruding exposed cylindrical carbon fiber, ~200 μm in length and 5 μm in diameter, of the carbon fiber microelectrodes was manually inserted into the edge of the blue region of a butane flame for about 2 s while rotating the electrode to ensure an even etching (Fig. 1B). As soon as the tip of the carbon electrode surface turned red, the electrode was quickly removed out of the flame, and the newly formed CFNE was inspected under the microscope to ensure successful fabrication.

2.3.4. Heat etching of carbon fiber microelectrodes into conical CFNEs

To fabricate heat-etched CFNEs, epoxy-insulated cylindrical microelectrodes with ~200 μm protruding exposed carbon fiber were fixed into position using a micromanipulator and brought to the edge of a 2.5 mm × 2.5 mm metal (90 %Pt/10 %Ir) box-shaped heating filament (Cat. # FB255B, Sutter Instruments Co., Novato, USA) of a micropipette puller (P-1000, Sutter Instruments Co., Novato, USA) powered by 220–240 V AC., 50 Hz line voltage (Fig. 1C). With the help of the micromanipulator, the tip of a carbon fiber microelectrode was positioned at ~1 mm from the heating mantle in both horizontal and vertical directions (as shown in schematic Fig. 1C and Fig. S1). Here, the position of the electrode tip with respect to the heating mantle is important to get a reproducible CFNE length and tip diameter. First, a Ramp test was performed according to manufacturer's instructions. This test determines the minimum heat required to soften borosilicate glass (typically above 820 °C) and depends on both type of glass capillary and the heating filament used. A Ramp value of 496 was obtained and the Heat value, which depends on the RAMP value, was optimized, with a value of 510 providing the best results. The puller applies current to the filament to rapidly reach temperatures sufficient to melt borosilicate glass capillaries, which is estimated to be around 1000 °C, within approximately 2 s. Cooling occurs rapidly and aided by the micropipette puller's internal air-cooling system, which is controlled by the time setting, which was set to 200. After subjecting the electrodes to the pre-programmed heat pulse by the filament, the heat-etched electrodes were inspected under a microscope to ensure the successful formation of a nanotip with the desired length.

2.4. Characterization of CFNEs using cyclic voltammetry

All etched CFNEs were tested by performing cyclic voltammetry in a 1 mM FcMeOH solution and scanning the voltage between −0.2 V and +0.8 V versus a saturated Ag/AgCl (3 M KCl) reference electrode at a 0.1 Vs^{-1} scan rate using a computerized multi-channel potentiostat (1030C, CH Instruments, USA). The cyclic voltammetry experiments were performed to make sure the etched CFNEs are well-functioning and showing stable steady-state current with the expected current amplitudes. Only such well-functioning electrodes were used for further experiments.

2.5. Electrode sensitivity measurements for neurotransmitters

Stock solutions (200 μM) of the different neurotransmitters: dopamine, norepinephrine, epinephrine, and serotonin, were prepared in 50 ml Milli-Q water. These stock solutions were diluted with 0.1 M phosphate buffer of pH 7.4 to obtain neurotransmitter sample solutions at desired concentrations, each with a final volume of 5 ml. Cyclic and square wave voltammograms were then recorded using a computerized multi-channel potentiostat. Square wave voltammetry (SWV) was performed using the following optimized parameters: initial potential (E_i) of −0.1 mV, final potential (E_f) of 600 mV, square wave amplitude (E_{sw}) of 25 mV, potential step (E) of 4 mV, and a frequency (f) of 15 Hz. All potentials are referenced against an Ag/AgCl electrode at an ambient temperature of 25 ± 2 °C. To prevent oxidation of the neurotransmitter samples by dissolved oxygen, nitrogen gas was bubbled through the testing solutions for 10 min prior to measurements.

2.6. Cell culture of SH-SY5Y cells

SH-SY5Y cells were cultured in DMEM/F12 with Glutamax™ (Fisher Scientific, Pittsburgh, PA) supplemented with 10 % fetal bovine serum (Sigma-Aldrich, St. Louis, MO) at 37 °C with 5 % CO_2 and high humidity. The cells were passaged upon reaching 80 % confluency using trypsin-EDTA (Sigma-Aldrich, St. Louis, MO). The cells were seeded onto 35 mm MatTek dishes with glass coverslip bottoms (MatTek, Ashland, MA) at a density of 5000 cells/cm^2 one day before experiments.

2.7. Single-cell intracellular amperometry at SH-SY5Y cells

Single-cell intracellular amperometry experiments were performed on sparsely cultured SH-SY5Y cells after three washes with warm isotonic HEPES buffer (10 mM HEPES, 1.2 mM $MgCl_2$, 2 mM $CaCl_2$, 150 mM NaCl, 5 mM KCl, and 5 mM glucose, pH 7.4, osmolality of 315 mOsm/kg). During the experiments, the cells were immersed in approximately 2 mL of the isotonic buffer. The culture dish was placed on the stage of an inverted microscope (Leica DM IRB, Leica Microsystems, Germany) inside a Faraday cage, with the temperature maintained at approximately 31 °C. Heat-etched CFNEs with an exposed carbon fiber tip of approximately 10 μm in length, backfilled with 3 M KCl, was connected to the head stage of a patch clamp amplifier and lowered onto a single cell using a micromanipulator. The sharp tip of the CFNE was then gently pressed against the cell membrane to perform insertion into the cell cytoplasm. After proper insertion, a constant potential of +800 mV was applied to the electrode surface versus a chloridized silver wire reference electrode, as this potential is sufficient to electrochemically oxidize the neurotransmitters, enabling their

detection as oxidation current. Data acquisition was performed using Axoscope 11.2 software (Molecular Devices, San Jose, CA) with a sampling rate of 20 kHz and using a 1 kHz internal lowpass Bessel filter and scaled out at 0.5 mV/pA. The release of norepinephrine from individual large dense core vesicles was detected as positive current spikes.

2.8. Data analysis

Amperometric current versus time traces were analyzed using Igor Pro 6.3 (WaveMetrics, Lake Oswego, OR) and a macro developed by David Sulzer's laboratory [37]. The traces were smoothed using a binomial smoothing filter at 5 kHz. As the cut-off threshold for automated spike detection, a threshold of five times the standard deviation of the background noise was chosen, followed by manual inspection and the removal of false positives. The important parameters obtained from the amperometric current spikes include the I_{max}, which is the highest amplitude of the current; the total charge Q per event, which is calculated by integrating the area under the spike; the temporal parameters $T_{1/2}$, which is the spike half-width at 50 % of I_{max}; the T_{rise}, which describes the rise time for the current from 25 % to 75 % of I_{max}; and T_{fall}, which describes the fall time from 75 % to 25 % of I_{max}.

3. Results and discussion

In this work, we developed an easy-to-use method utilizing heat etching of carbon fiber microelectrodes for fabricating CFNEs. This method enables the production of highly sensitive electrodes with precise dimensions and electrochemical properties suitable for intracellular neurotransmitter measurements and neurotransmission recordings near neuronal synapses. Our goal was to develop a technique that offers improved control over CFNE fabrication with higher reproducibility and greater success rate while allowing the fabrication of significantly shorter electrode tips (<10 μm in length) compared to existing fabrication methods.

3.1. Fabrication of heat-etched CFNEs

To explore heat etching as a method for creating nanoelectrodes, we used a micropipette puller equipped with a time- and temperature-controlled metal heating filament as the heat source. Since temperature, duration and electrode distance to the heat source all play crucial roles in affecting CFNE dimensions, the position of the glass-insulated carbon fiber microelectrodes was fixed at a constant distance, 1 mm away (both vertically and horizontally) from the center of the heating filament using a micromanipulator (Fig. S1B). The etching process was optimized by systematically varying the temporal and thermal heating parameters of the micropipette puller and subjecting the carbon fiber to programmed heat pulses by the heating filament. The resulting electrode shape and its dimensions were initially inspected under an upright light microscope and further analyzed using FE-SEM imaging to determine the optimal heat pulse settings for heat etching.

Our findings showed that setting a heat value of 510 on the Sutter Instruments P-1000 micropipette puller, reaching estimated temperatures of around 1000 °C within 2 s, consistently produced cone-shaped CFNEs with sharp electrode tips about 100 nm in diameter. However, these parameter settings are unique to the specific micropipette puller and may be affected by factors such as the condition of the metal heating filament since its shape can be altered from use over time or minor dents during replacement. Therefore, thorough visual inspection of fabricated electrodes is recommended between production batches, as minor defects on the heating filament may necessitate slight alterations to the heat etching parameters. Although tests were performed exclusively using a P-1000 micropipette puller, the method should be transferable to other heat-based glass micropipette pullers. Since the filament in such devices provides extremely rapid heating (~500 °C/s) and cooling, it offers a unique advantage over non-filament-based heating systems. However, adapting the method to other devices would require extensive optimization of all parameters, due to differences in the heating and cooling rates as well as maximum achievable temperatures. To compare the electrode surface characteristics and electrochemical properties of CFNEs created from heat etching with those produced using conventional electrochemical and flame etching methods, all CFNEs were fabricated with a standard length of 100 ± 10 μm. Electrodes from all three fabrication methods were characterized through visual inspection methods and electrochemical analysis.

3.1.1. Analysis of CFNE geometry and size using FE-SEM imaging

To compare the tip geometry and final dimensions of the CFNEs fabricated using the three different etching methods, FE-SEM imaging was performed for individual electrodes. All three fabrication methods resulted in the formation of sharp cone-shaped electrodes. Image analysis of the FE-SEM images was performed to measure the diameter at the base of the cone-shaped electrode and at the tip. These dimensions were further used to calculate the final electrode area, *A*, of the etched bare carbon nanotip, according to the area equation for a cone: $A = \pi (r + R) ((R - r)^2 + l^2)^{1/2} + \pi r^2$, where *r* is the tip radius, *R*, is the radius of the carbon fiber at the glass seal, and *l* is the length of the electrode [29]. The average diameters of the carbon electrodes at the glass-carbon fiber junction are summarized in Fig. 2.

3.2. FE-SEM imaging shows heat etching creates rich nanostructured carbon surfaces

To examine the surface morphologies of heat-etched CFNEs and compare them to the surface properties of electrodes fabricated using conventional electrochemical and flame etching, Field-Emission Scanning Field Microscopy (FE-SEM) micrographs of the CFNEs surfaces were recorded (Fig. 3). In general, the electrochemically etched CFNEs exhibited a very smooth surface (Fig. 3D, G, 3J), while high magnification images of the flame-etched CFNEs revealed sparse bumps and nanostructured features at the carbon fiber surface (Fig. 3H and K). However, in comparison to electrochemical etching and flame etching, micrographs of heat-etched CFNEs showed a significantly rougher nanostructured surface (Fig. 3I and L). Nanostructured roughness was observed along the entire conical surface of the electrode, from its base (Fig. 3F) to the tip (Fig. 3L). SEM images revealed a predominance of nanostructured carbon dots at the electrode tip, where heat exposure is the most intense during etching, while the upper region of the carbon fiber located farther from the heat source, exhibited a higher density of nanocavities. This gradient in nanostructure distribution results in a highly porous electrode surface. From these FE-SEM micrographs, it was concluded that electrochemically etched electrodes have a smoother surface, flame-etched electrodes have a low density of small bumps, and heat-etched electrodes show defect-rich surfaces with high surface roughness, with the tip enriched in nanodots and the upper shaft characterized by nanocavities. A FE-SEM micrograph of bare carbon fiber is shown in Fig. S2 (Supporting Information).

3.3. EDX imaging shows that heat etching creates oxygen-rich carbon surfaces

To analyze how the surface chemistry of the CFNEs fabricated using the three different etching methods is affected, the relative presence and surface distribution of oxygen were analyzed using energy dispersive X-ray spectroscopy (EDX). Each newly fabricated CFNEs were analyzed at three specific regions of interest: at the edge where the glass seal meets the bare carbon fiber, at the electrode tip, and at a spot in between the glass edge and the electrode tip. Measurements of the atomic percentage (at. %) were performed on the carbon surface of the CFNEs fabricated using electrochemical etching ($n = 5$), flame etching ($n = 5$), and heat etching ($n = 5$) (Fig. 4). Analysis of the intensity of the elemental spectroscopic peak for oxygen from the EDX data for the three types of

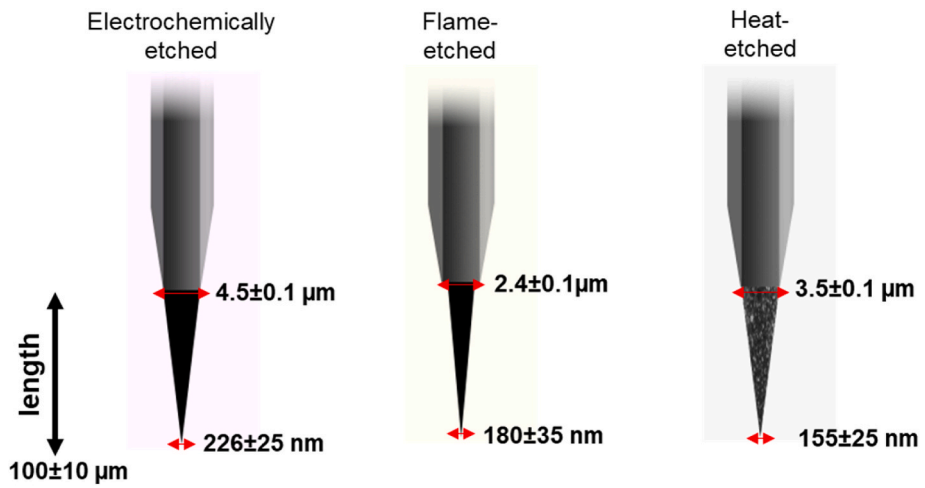

Fig. 2. A schematic of the geometrical shape and dimensions of CFNEs fabricated by electrochemical etching, flame etching and heat etching showing the mean measured diameter ± S.E.M. Measurements were performed on the FE-SEM images of electrodes at two regions 1) at the glass-carbon fiber junction and 2) at the tip of the electrode. Schematics are not drawn to scale. n = 14 for electrochemically etched electrodes, n = 19 for flame-etched electrodes, and n = 22 for heat-etched electrodes.

CFNEs showed a clear difference. On average, electrochemically etched CFNEs had an oxygen level of 0.6 ± 0.07 at. % at the midway point of the exposed carbon fiber tip, which increased to 1.1 ± 0.2 at. % at the tip of the electrode, while the average atomic presence of oxygen at flame-etched carbon surfaces was 0.4 ± 0.07 at. % at the midway point and increased to 0.8 ± 0.2 at. % at the electrode tip. Compared to the electrochemically- and flame-etched carbon surfaces, the heat-etched CFNE surface had a significantly higher level of atomic oxygen, with an average of 2.5 ± 0.6 at. % at the midway point between the glass junction and the very tip (One-way ANOVA with Tukey test, $p = 0.006$ for electrochemically etched versus heat-etched CFNE and $p = 0.003$ for flame-etched versus heat-etched CFNE), which increased to 4.4 ± 1.2 at. % at the electrode tip (One-way ANOVA with Tukey test, $p = 0.017$ for electrochemically etched versus heat-etched CFNE and $p = 0.010$ for flame-etched versus heat-etched CFNE). Clearly, the maximal presence of at. % oxygen groups were found at the tip of all three types of CFNEs, a site where all three etching processes are the most effective. The abundance of oxygen groups on the heat-etched carbon fiber surface suggests defective sites or edge plane sites by oxygen functional groups as previously observed at the carbon nanotube fiber cross-section [38] Click or tap here to enter text. The EDX graphs are shown in Fig. S3, S4 and S5 (Supporting Information).

3.4. Characterizing the carbon surface of CFNEs using Raman spectroscopy

To characterize the surface structure of CFNEs and to identify the relative presence of graphite-type lattice produced by the three etching methods, Raman spectroscopy was performed. Ordered graphite-type lattice is indicated by the intensity of the G band (I_G), corresponding to the vibrational signals from its sp^2 carbon, while disordered graphite-type lattice is indicated by the intensity of the D band (I_D), corresponding to the signal from the sp^3 carbon. Raman spectroscopy was performed using a 532 nm laser with a 0.7 µm spot size and 1 % power attenuation. Spectra were acquired from different positions (n = 5, 20 s acquisition time) on electrochemical-, flame-, and heat-etched CFNEs (n = 5) and compared to the surface of untreated bare carbon fiber. The Raman spectra were fitted using the minimum number of required Lorentzian peaks. For bare carbon fiber, two characteristic peaks were observed: the D band at 1370 and the G band at 1594 cm^{-1}. An additional peak at ~1522 cm^{-1} was also detected, which may be attributed to amorphous carbon (AC) or specific functional groups [39,40]. For the electrochemical-, flame- and heat-etched CFNEs, the D and G band positions shifted to 1352 cm^{-1}, 1356 cm^{-1}, 1355 cm^{-1} (D band) and 1587 cm^{-1}, 1586 cm^{-1}, 1591 cm^{-1} (G band), respectively, indicating a red shift (Fig. 5). The AC-related peak appeared at 1517 cm^{-1}, 1520 cm^{-1} and 1526 cm^{-1} for electrochemical-, flame- and heat-etched CFNEs, respectively. The full width at half maximum (FWHM) of the D band increased modestly to ~8 cm^{-1} for electrochemically etched CFNEs and ~18 cm^{-1} for flame-etched CFNEs. In contrast, heat-etched CFNEs showed a substantial increase in D-band FWHM to ~40 cm^{-1}, indicating a significantly higher degree of surface defects [40]. The FWHM of the G and AC bands showed smaller variations across the different types of etched electrodes ranging from ~5 to 6 cm^{-1}. The integral area ratio of the D band to the G band (I_D/I_G) commonly used to quantify disorder in carbon materials, was highest for heat-etched carbon fibers (~3.4), compared to ~2.68 and ~2.8 for electrochemically and flame-etched fibers, respectively. The substantial increase in the D/G ratio after heat-etching likely reflects the increased surface roughness and higher density of surface defects, consistent with FE-SEM images (Fig. 3I and L), which show more defect-rich surface morphology. Additionally, the integral area ratio of the AC to G band (I_{AC}/I_G), used to assess the presence of amorphous carbon, decreased from 0.7 for bare carbon fiber to 0.4, 0.6, and 0.5 for electrochemical-, flame-, and heat-etched carbon fibers, respectively. This trend indicates a reduction in amorphous carbon content following the etching process [39]. Fig. S6 (Supporting Information) presents a comparative graph of the integral intensity ratios I_D/I_G and I_{AC}/I_G for bare, electrochemical-, flame- and heat-etched CFNEs.

3.5. Characterizing CFNEs using cyclic voltammetry

Cyclic voltammetry is a convenient electroanalytical technique used for qualitative analysis of redox processes, electron transfer kinetics, and reversibility of reactions. By scanning the potential while measuring the redox current and plotting the potential versus the current density in a cyclic voltammogram (CV), information about the magnitude of the current flowing per unit area of the electrode surface can be obtained. This can be used to characterize the sensitivity of the electrodes as well as other electrochemical properties. To investigate the background current of these electrodes, repeated CVs were recorded in the potential range of 0 mV–1000 mV in 0.1 M phosphate buffer at a scan rate of 100 mV/s using electrochemically (n = 5), flame- (n = 5), and heat-etched (n = 5) CFNEs versus Ag/AgCl reference electrode (Fig. 6A). To compare the magnitude of background current between the CFNEs, the average anodic and cathodic currents recorded at +0.5 V were calculated and

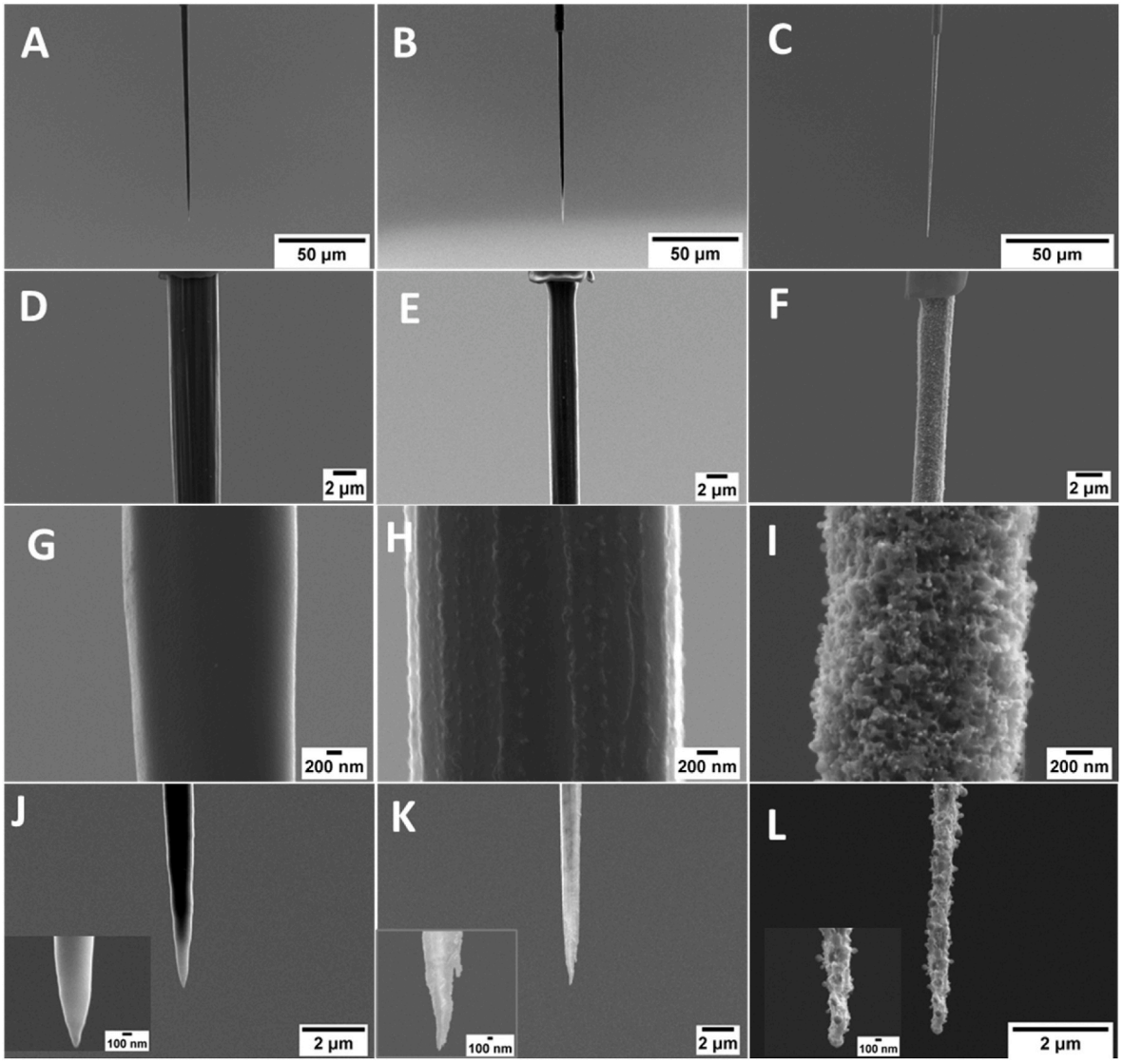

Fig. 3. FE-SEM micrographs of electrochemical- (A, D, G and J), flame- (B, E, H, and K) and heat- (C, F, I and L) etched CFNEs at different magnifications. A, B and C show the entire electroactive surface area from the pulled glass seal to the electrode tip for the three electrode types. D, E and F display the junction between the etched carbon fiber and the glass seal. G, H and I show a high-magnification image of the surface features of three electrode types. J, K and L show the tips of the three types of electrodes, with the insets showing close-ups of the nanotips.

normalized to the total electrode area, assuming a conical geometry (as detailed in Section 3.1.1**)**. Electrode areas were determined based on dimensions from FE-SEM images. The measured average background current for heat-etched electrodes (black CV) was 922 ± 110 pA, with a normalized current equaling 0.79 ± 0.08 pA/µm^2. The measured background current for flame-etched CFNEs (red CV) was 167.34 ± 10 pA, with a normalized current of 0.2 ± 0.01 pA/µm^2. Electrochemically etched CFNEs were found to have similar electrochemical properties as the flame electrodes, with a background current of 275 ± 40 pA and a normalized current of 0.18 ± 0.03 pA/µm^2 (blue CV) (One-way ANOVA with Tukey test, $p = 0.96$). Hence, flame-etched CFNEs showed slightly higher but statistically non-significant background current than electrochemically etched CFNEs (Fig. 6A inset). In comparison, heat-etched CFNEs demonstrated about four times higher background current than the CFNEs produced using the two alternative methods (One-way ANOVA with Tukey test, $p < 0.0001$ for electrochemically etched versus heat-etched CFNEs and $p < 0.0001$ for flame-etched versus heat-etched CFNEs). The significantly higher background current of the CVs recorded in phosphate buffer was indicative of electrode capacitance.

The capacitance, *C,* was calculated from the measured current results obtained with cyclic voltammetry using the formula $i = \nu C$, where *i* is the measured background current at 0.5 V, and *ν* is the scan rate, which was set to 100 mVs^{-1}. The calculated capacitance value was then divided by the geometric area of the CFNEs. The average capacitance value for heat-etched CFNEs was calculated to equal 789 ± 75 µF/cm^2, which was significantly higher than the values for flame-etched and electrochemically etched CFNEs which were estimated to be 198 ± 10 µF/cm^2 and 169 ± 25 µF/cm^2, respectively (One-way ANOVA with Tukey test, $p <$ 0.0001 for electrochemically etched versus heat-etched CFNEs and $p <$ 0.0001 for flame-etched versus heat-etched CFNEs). The four to five times higher capacitance for heat-etched electrodes might be related to their nanostructured electrode surface having a very high surface roughness, as confirmed by FE-SEM imaging, which significantly increases the total effective surface area of these electrodes.

To further investigate the sensitivity and electron transfer kinetics of the three CFNE types (n = 5 for each), cyclic voltammetry was performed using the redox probes FcMeOH, $Ru(NH_3)_6Cl_3$ and $K_3[Fe(CN)_6]$. Fig. 6B depicts representative CVs recorded at all three electrodes in 1 mM FcMeOH containing 0.1 M KCl at a scan rate of 10 mV/s. The CVs for the oxidation of $[FcMeOH]^+$ displayed sigmoidal steady-state CVs with

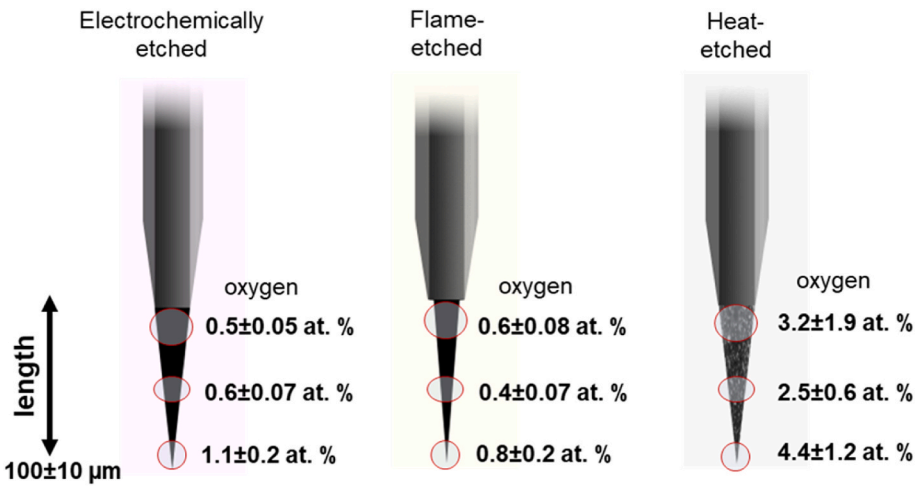

Fig. 4. A schematic showing the regions of interest analyzed using energy dispersive X-ray spectroscopy to determine the relative abundance of atomic oxygen at the carbon surface after electrochemical, flame and heat etching (values are expressed as at. % ± S.E.M.).

current densities in the picoampere range. Notably, the heat-etched electrodes demonstrated significantly higher sensitivity for the redox analyte compared to the other types of electrodes. This enhanced sensitivity is attributed to the highly nanostructured electrode surface composed of carbon nanodots and nanocavities that lead to a larger exposed electrode surface area. In contrast, electrochemically and flame-etched electrodes that are lacking this nanostructured surface resulted in a lower sensitivity. The steady-state current response indicated nonlinear diffusion behavior at the electrode surface. The half-peak potential used to calculate the rate of electron transfer kinetics indicated reversible and fast electron transfer kinetics at all three electrodes, as demonstrated by the narrow difference between the 1/4- and 3/4-wave potentials ($E_{3/4} - E_{1/4} \approx$ 59–60 mV, for all three electrodes). Although the capacitance of the heat-etched CFNE increased by more than fourfold, the oxidation current of FcMeOH increased by only about twofold. This disparity can be attributed to the fact that capacitive (non-Faradaic) current scales with total surface area, particularly in electrodes with rough or porous structures that act as ion-buffering reservoirs. Such surface features reduce the diffusion path length of ions, promoting rapid transport of electrolyte ions and solvent molecules, and thereby enhancing double-layer charging and discharging processes. However, not all of the additional surface area is electrochemically accessible for Faradaic reactions. Diffusion limitations within deeper pores or crevices can restrict analyte access and hinder electron transfer, effectively reducing the electroactive area. As a result, the Faradaic (oxidation) current of FcMeOH does not increase proportionally with capacitance [41–43].

Although the FcMeOH/$[FcMeOH]^+$ redox couple is typically surface-insensitive and exhibits outer-sphere electron transfer, the enhanced sensitivity at the heat-etched electrode surface may likely be due to π-π and CH-π interactions between the cyclopentadienyl rings in FcMeOH and the graphitic carbon surface, where polar groups on the carbon facilitate CH-π and hydrogen bonding interactions [44,45]. EDX analysis revealed a higher percentage of oxygen functionalities on the heat-etched CFNE surface, which can favor hydrogen bonding interactions with FcMeOH molecules. The observed hysteresis in the cyclic voltammograms recorded with heat-etched CFNEs can be attributed to the electrochemical double-layer charging and discharging. The reproducibility of the heat-etched electrode fabrication was confirmed by obtaining overlapping CVs (n = 5) for FcMeOH, as shown in Fig. S7.

Fig. S8A and S8B show the CVs recorded for $Ru(NH_3)_6Cl_3$ and $K_3[Fe(CN)_6]$ using the different types of CFNEs. The steady-state CVs observed for $Ru(NH_3)_6^{3+/2+}$, an outer-sphere redox couple insensitive to surface electrocatalytic effects, showed consistent electrochemical behavior across all three electrodes. Specifically, the difference between the 1/4- and 3/4-wave potentials ($E_{3/4} - E_{1/4}$) was approximately 59–60 mV for all three electrodes. The slight variations in current densities are attributed to differences in active surface area caused by surface roughness at the flame and heat-etched electrodes (Fig. S8A). In contrast, the CVs recorded in $Fe(CN)_6^{3-/4-}$, an inner-sphere redox couple highly sensitive to surface functionalities on the carbon surface, showed sigmoidal-shaped CVs with irreversible and slow electron transfer kinetics (Fig. S8B). Although $Fe(CN)_6^{3-/4-}$ is often used to characterize various electrode surfaces, it is also known to exhibit complex and non-ideal redox behavior due to the adsorption of ferricyanide decomposition species on the electrode surface. This adsorption effect hinders the electron transfer kinetics, particularly at carbon surfaces [38].

3.5.1. *Cyclic voltammetric detection of neurotransmitters*

The sensitivities of the CFNEs fabricated using the three etching methods were evaluated for the detection of four different neurotransmitters: dopamine, epinephrine, norepinephrine, and serotonin, using cyclic voltammetry and square wave voltammetry. To ensure a fair comparison of sensitivities, all CFNEs electrode were fabricated with the same length (100 ± 10 μm) and a similar total electrode surface area.

3.5.1.1. Dopamine. Characterization of the three CFNE types for dopamine detection was performed using cyclic voltammetry in 5 μM dopamine dissolved in 0.1 M phosphate buffer at pH 7.4. The applied potential was scanned between −0.2 V and +0.6 V against an Ag/AgCl reference electrode at a scan rate of 100 mV/s. All three electrodes exhibited well-defined anodic and cathodic peaks corresponding to the oxidation of dopamine to o-dopamine-quinone and reduction back to dopamine, respectively (Fig. 7A). The heat-etched electrode displayed a well-defined reversible redox couple reaction for dopamine, with oxidation and reduction peaks at ~162 mV and ~132 mV respectively, resulting in a peak potential separation (Δ*E*p) of ~30 mV. In contrast, the CVs recorded for flame- and electrochemically etched CFNEs showed quasi-steady-state behavior, suggesting non-transient processes. The half-peak potential ($E_{1/4} - E_{3/4}$) was ~30 mV (Fig. 7A), confirming reversible two-electron oxidation of dopamine with fast electron transfer at all three types of CFNEs. The oxidation peak current densities were 0.35 ± 0.05 pA/μm^2, 0.19 ± 0.04 pA/μm^2 and 0.12 ± 0.02 pA/μm^2, for heat-etched, flame-etched, and electrochemically etched electrodes, respectively.

To investigate the electron transfer pathway involved in the electrochemical redox process of dopamine at these three types of CFNEs, cyclic voltammetry was performed over a range of scan rates from 10 to 1000 mV/s. At slow scan rates, both the electrochemically and the

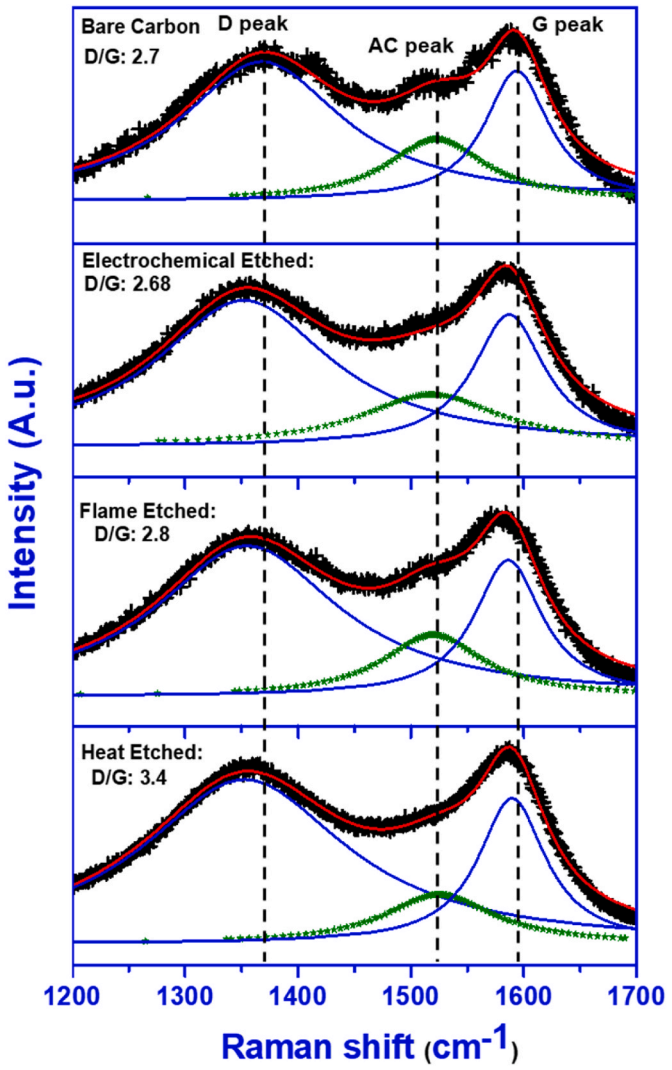

Fig. 5. Raman spectra of bare carbon fiber (top), electrochemically etched (second from top), flame-etched (second from bottom), and heat-etched (bottom) CFNEs. In the graph, raw data are represented by + symbols (black line), the cumulative fit is shown as a red solid line, individual Lorentzian fits are shown as blue solid lines and amorphous carbon (AC) is shown as an olive star line. (For interpretation of the references to colour in this figure legend, the reader is referred to the Web version of this article.)

flame-etched CFNEs showed steady-state or sigmoidal CVs, characteristic of radial diffusion at conical geometries. As the scan rates increased beyond 50 mV/s, the CVs transitioned from radial to semi-infinite linear diffusion, as evidenced by peak shape [46–48] (Fig. 7B and C). This shift reflects differences in mass transport dynamics within the diffusion layer at lower vs higher scan rates. The increase in the scan rates also caused the oxidation peak potential to shift positively and the reduction peak negatively, consistent with the behavior of heterogeneous kinetic control. Correspondingly, the peak-to-peak separation (ΔEp) increased from ~30 mV at low scan rates, indicating near-ideal reversibility, to ~64 mV at the highest scan rate (1000 mV/s) reflecting a shift toward irreversible dopamine oxidation (Fig. 7B and C). Additionally, pronounced hysteresis was observed during the reverse scan which may be caused by electrochemical double-layer charging and discharging. The heat-etched CNFEs displayed steady-state CVs at 10 mV/s. At scan rates above 50 mV/s, well-defined oxidation and reduction peaks emerged, with peak currents increasing linearly with scan rate. Notably, peak potential shifts were minimal, and ΔEp for dopamine remained close to 30 mV up to 500 mV/s. At 1000 mV/s, ΔEp increased slightly to ~35 mV, indicating a transition from reversible to quasi-reversible behavior at high scan rates (Fig. 7D). The enhanced sensitivity (i.e. higher current density) and faster electron transfer kinetics (i.e. lower value of ΔEp) observed for the heat-etched electrodes can be attributed to the nanostructured surface roughness and the presence of graphitic defects or edge plane sites. For all three electrode types, the anodic peak current (i_p) increased linearly with of scan rate ($\nu^{1/2}$) and dopamine concentration, as described by the following equations.

Electrochemically-etched CFNEs:

$i_p = (4.887E\text{-}4 \pm 2.94E\text{-}5)\ (\nu/\ mV/s) + (0.1278 \pm 0.0150)\ R^2 = 0.988$

$i_p = (0.0193 \pm 8.19E\text{-}4)\ (\nu^{1/2}/\ mV/s)\ \text{-}\ (0.0202 \pm 0.0157)\ R^2 = 0.996$

$Log(i_p) = (0.511 \pm 0.0192)\ log(\nu/\ (mV/s))\ \text{-}\ (1.7716 \pm 0.0459)\ R^2 = 0.995$

Flame-etched CFNEs:

$i_p = (0.0011 \pm 1.12E\text{-}4)\ (\nu/\ mV/s) + (0.2812 \pm 0.0570)\ R^2 = 0.969$

$i_p = (0.0438 \pm 0.0012)\ (\nu^{1/2}/\ mV/s)\ \text{-}\ (0.0600 \pm 0.0227)\ R^2 = 0.997$

$Log(i_p) = (0.594 \pm 0.0164)\ log(\nu/\ (mV/s))\ \text{-}\ (1.534 \pm 0.0393)\ R^2 = 0.996$

Heat-etched CFNEs:

$i_p = (0.0015 \pm 1.54E\text{-}4)\ (\nu/\ mV/s) + (0.3341 \pm 0.0788)\ R^2 = 0.967$

$i_p = (0.0583 \pm 5.24E\text{-}4)\ (\nu^{1/2}/\ mV/s)\ \text{-}\ (0.1208 \pm 0.0101)\ R^2 = 0.999$

$Log\ (i_p) = (0.518 \pm 0.0338)\ log(\nu/\ (mV/s))\ \text{-}\ (0.1343 \pm 0.0749)\ R^2 = 0.997$

The linear dependence of i_p vs. $\nu^{1/2}$ (shown in the insets of Fig. 7B, C and 7D) and log i_p vs. log ν having a slope value below or near to ~0.5 confirms that the oxidation of dopamine proceeds via a diffusion-controlled process at higher scan rates. At 10 mV/s, CV feature was a sigmoidal steady state; therefore, only the recorded data from CVs obtained with scan rates ranging between 50 mV/s to 1000 mV/s were used to plot the graph of scan rate vs. anodic peak current amplitude.

Electrochemical characterizations of electrochemically, flame- and heat-etched CFNEs for the detection of epinephrine, norepinephrine, and serotonin were also carried out in a similar way (Section 7, supporting information). Cyclic voltammetry data revealed that heat-etched electrodes offered a significantly higher sensitivity over electrochemically and flame-etched electrodes for epinephrine (Fig, S9), norepinephrine (Fig. S10), and serotonin (Fig. S11) detection as well. To elucidate the nature of the electron transfer process, the effect of scan rate ranging from 10 to 1000 mV/s on the peak current was also studied. Similar to dopamine at slow scan rates, the oxidation of epinephrine and norepinephrine at all three electrodes showed ideal reversible behavior. With the increase in scan rates, the peak-to-peak separation (ΔEp) increased from ideal reversibility at slow scan rates to irreversible at fast scan rates (1000 mV/s) for electrochemically and flame-etched electrodes, while the peak shifting was not significant in the case of heat-etched electrodes at higher scan rates, thus showed quasi-reversible nature. The linear dependence of i_p on $\nu^{1/2}$ confirmed that the oxidation of epinephrine and norepinephrine follows a diffusion-controlled pathway at all three electrodes. The scan rate experiment for serotonin revealed irreversible oxidation of serotonin at the three CFNE surfaces, with the current versus scan rate plot indicating that the electron transfer reaction was a mixture of diffusion- and adsorption-controlled processes.

3.6. *Testing the sensitivity of CFNEs using square-wave voltammetry*

Square wave voltammetry (SWV) subtracts non-faradaic charging current and therefore shows higher sensitivity compared to cyclic

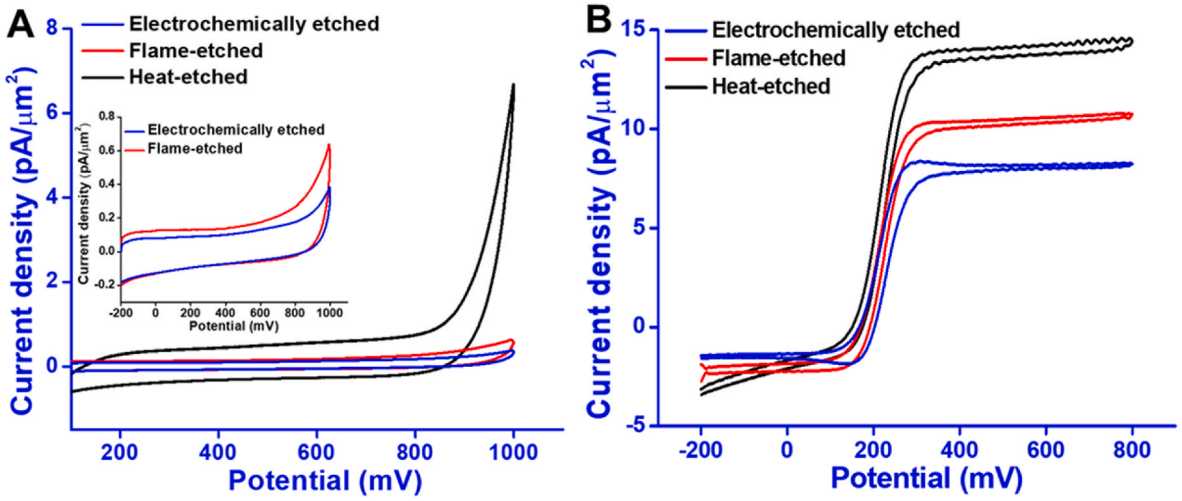

Fig. 6. Cyclic voltammograms from recordings of electrochemical, flame-, and heat-etched CFNEs (A) in 0.1 M phosphate buffer at a scan rate of 100 mV/s versus Ag/AgCl reference electrode (inset shows a voltammogram recorded on electrochemically etched and flame-etched electrodes); and (B) in 1 mM FcMeOH containing 0.1 M KCl at a scan rate of 10 mV/s versus Ag/AgCl reference electrode.

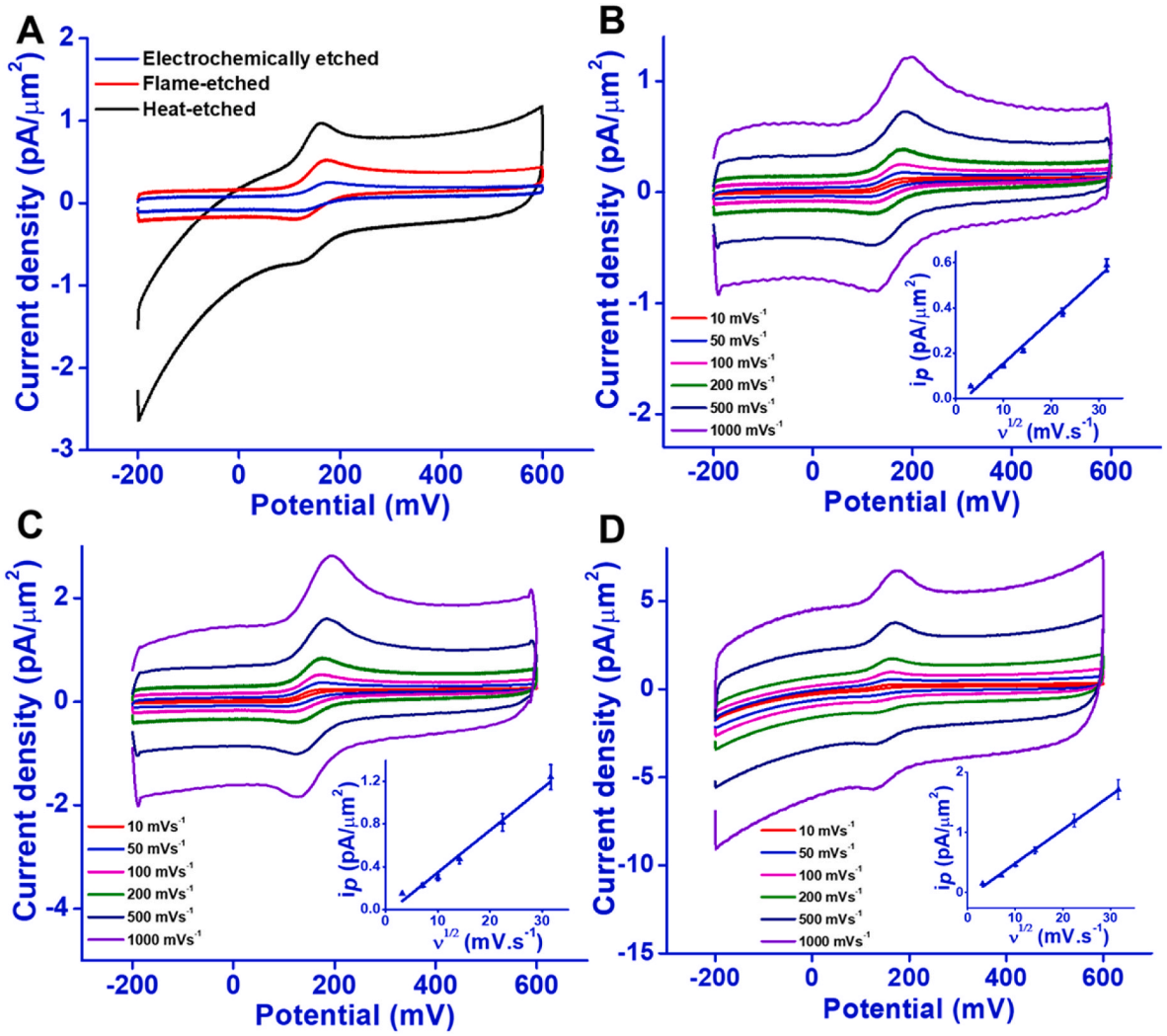

Fig. 7. Cyclic voltammetry analysis of CFNE sensitivity for dopamine. (A) A comparison of CVs recorded at electrochemically, flame- and heat-etched CFNEs in 5 μM dopamine dissolved in phosphate buffer of pH 7.4 at a scan rate of 100 mV/s against Ag/AgCl reference electrode. CVs of 5 μM DA in phosphate buffer of pH 7.4 with increasing scan rates and in a range of 10–1000 mV/s at (B) electrochemical, (C) flame- and (D) heat-etched CFNEs. Inset is the linear relationship graph between the oxidation peak current amplitude (i_p) vs. scan rate ($\nu^{1/2}$). $n = 3$ electrodes for each type of CFNE.

voltammetry. The SWV experiments were performed in 5 μM dopamine (in 0.1 M phosphate buffer, pH 7.4) to compare the sensitivity of the three types of CFNEs (Fig. 8A). A well-defined oxidation peak for dopamine was observed for the heat-etched CFNEs when applying a 150 mV and a 157 mV potential to electrochemically and flame-etched electrodes versus a Ag/AgCl reference electrode. A remarkable increase in the dopamine oxidation peak current was observed at the heat-etched electrode surfaces, where the current density was ~5 times higher than the value at the electrochemically and flame-etched electrodes. From these observed results, it can be concluded that the greater sensitivity of heat-etched electrodes relates to the electrochemical properties of the exposed graphitic edge plane sites at the highly nanostructured rough surface that electrocatalyze the dopamine oxidation. In contrary, the lower abundance of such edge plane sites and absence of nanostructured rough surfaces resulted in a lower sensitivity for electrochemically and flame-etched electrodes.

To further investigate the effect of dopamine concentration on the peak current, dopamine quantification was carried out at the three types of CFNEs using SWV with increasing concentrations of dopamine prepared in 0.1 M sodium phosphate (pH 7.4). Upon spiking the solution with 100 nM dopamine, the oxidation peak recorded at 148 mV (vs Ag/AgCl reference electrode) by the heat-etched electrode further developed into a well-defined, enhanced peak current (Fig. 8D). The anodic peak current response increased noticeably with increasing dopamine concentration, as shown in the insets.

The dependence of anodic peak current on dopamine concentration was found to have two linear ranges for electrochemically, flame- and heat-etched CFNEs (Fig. 8B–D), which can be expressed by the following equations:

Electrochemically etched CFNE:

$$i_p\ (\text{nA}) = 0.0938[C_{\text{dopamine}}(0.1\text{–}1\ \mu\text{M})] + 0.0122\ R^2 = 0.983$$

$$i_p\ (\text{nA}) = 0.0397[C_{\text{dopamine}}(1\text{–}10\ \mu\text{M})] + 0.0872\ R^2 = 0.989$$

Flame-etched CFNE:

$$i_p\ (\text{nA}) = 0.1283[C_{\text{dopamine}}(0.1\text{–}1\ \mu\text{M})] + 0.0579\ R^2 = 0.982$$

$$i_p\ (\text{nA}) = 0.0417[C_{\text{dopamine}}(1\text{–}10\ \mu\text{M})] + 0.1613\ R^2 = 0.986$$

Heat-etched CFNE:

$$i_p\ (\text{nA}) = 0.5243[C_{\text{dopamine}}(0.1\text{–}1\ \mu\text{M})] + 0.0492\ R^2 = 0.986$$

$$i_p\ (\text{nA}) = 0.1861[C_{\text{dopamine}}(1\text{–}10\ \mu\text{M})] + 0.4160\ R^2 = 0.997$$

where i_p is the peak current response and C_{dopamine} is the dopamine concentration in μM. The limit of detection (L.O.D), calculated by $3\sigma/b$ where σ is the standard deviation of the blank solution and b is the slope of the calibration curve, for dopamine at electrochemically, flame- and heat-etched electrodes was determined to be 35 nM, 20 nM, and 8 nM, respectively. The sensitivity, expressed as the current density (current divided by the electrode surface area), was five times higher for heat-etched electrodes than for flame- and electrochemically etched electrodes. The reduced sensitivity at higher concentrations can be attributed to the adsorption of dopamine and intermediate products at the active sites on the CFNE surfaces.

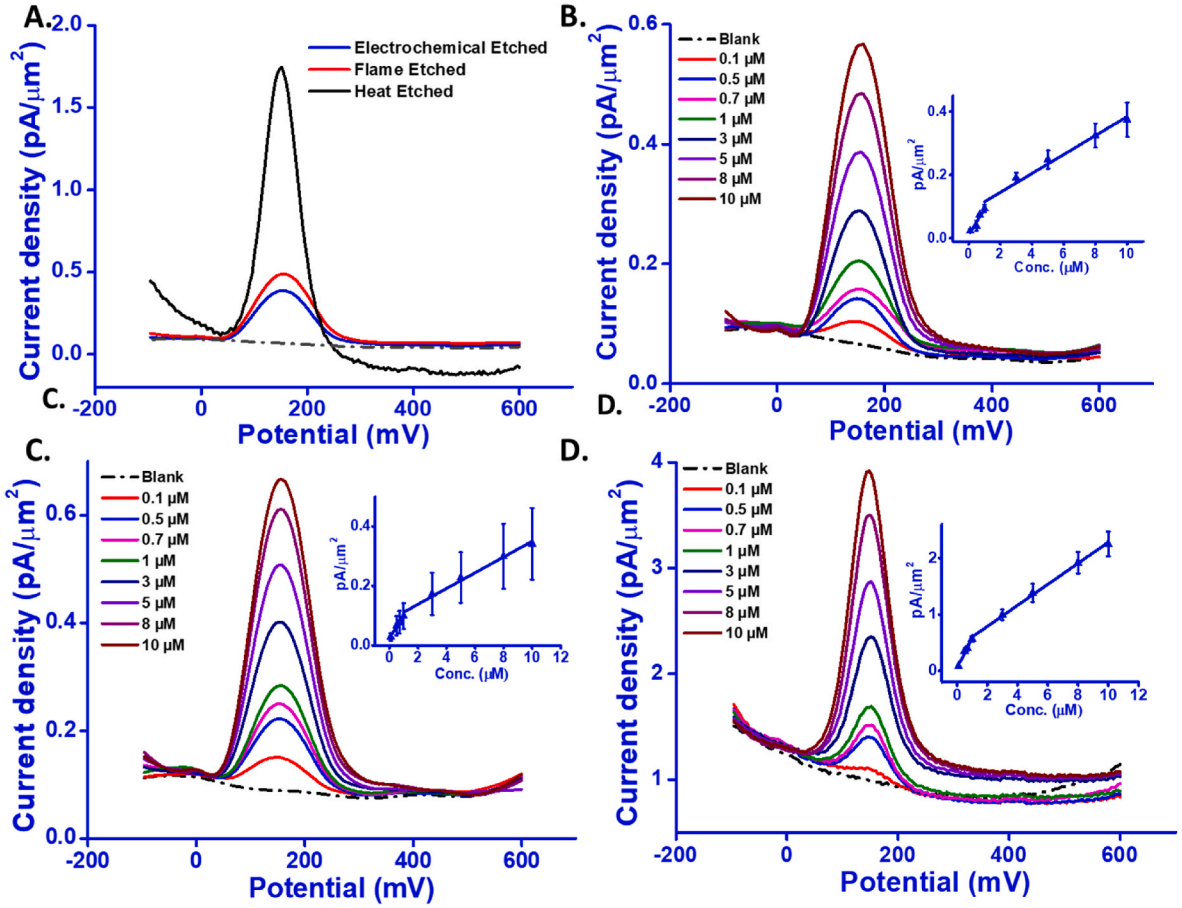

Fig. 8. Characterization of CFNE sensitivity using SWV. (A) SWVs obtained for 5 μM dopamine in phosphate buffer of pH 7.4 at electrochemically, flame- and heat-etched electrodes. SWVs recorded at (B) electrochemically, (C) flame- and (D) heat-etched CFNEs in 0.1 M phosphate buffer of pH 7.4 (dash line) and increasing concentration of dopamine (solid line). Insets are the corresponding linear calibration plots. $n = 3$ electrodes for each type of CFNE.

3.7. Resistance to chemical fouling

To evaluate the resistance of electrochemically, flame-, and heat-etched CFNEs against chemical fouling by dopamine, steady-state amperometric measurements were conducted at a working potential of +0.8 V *vs* Ag/AgCl (3 M KCl) in a 200 μM dopamine solution (in phosphate buffer, pH 7.4) (Fig. 9). Heat-etched CFNEs exhibited significantly greater stability against fouling caused by the neurotransmitter's oxidation products, which can be attributed to the abundance of defective graphitic sites-an observation also supported by Raman spectroscopy. These electrodes nearly maintained their initial steady-state current for ~30 min, whereas electrochemically and flame-etched CFNEs displayed a continuous decline in signal from the outset, with an approximately 50 % decrease under identical conditions (at 2000 s, $p = 0.0035$ for heat-etched vs. electrochemically etched CFNE, $p = 0.003$ for heat-etched vs. flame-etched CFNEs, one-way ANOVA, post-hoc Tukey test, $n = 3$). After 1 h of continuous oxidation of 200 μM dopamine, the current dropped by only 30 % for heat-etched CFNEs, compared to a reduction of over 85 % for electrochemically and flame-etched CFNEs. Initial currents values in the raw data were in the nanoampere range, with a 1–2 nA difference. However, due to the presence of signal noise during the early phase of the experiment, and a selection of discrete time points for plotting, followed by normalization, the starting points in the plotted graph appear nearly identical across all three electrode types (Fig. S12).

3.8. Neurotransmitter analysis in cerebrospinal fluid

In recent decades, carbon fiber has become the gold standard material for microelectrodes in *in vivo* or *in situ* monitoring of neurotransmission using techniques such as cyclic voltammetry and amperometry. However, carbon fiber electrodes are prone to fouling due to the adsorption of neurotransmitter oxidation products formed during electrochemical analysis as well as adsorption of proteins and other extracellular small molecules. Since the fouling of electrode surfaces significantly impacts measurement quality, carbon fiber microelectrode surfaces often are coated with carbon nanomaterials that enhance surface roughness and increase edge plane sites, which improve fouling resistance [6,13,17]. However, producing a uniform layer of carbon nanomaterials on a carbon fiber microelectrode surface is challenging and can also contribute to interference during measurements. Therefore, a few research groups have studied carbon nanotube fiber disk microelectrodes for electrochemical analysis of neurotransmitters and found that the defect sites significantly modulate the fouling effect [18,49,50]. The heat-etching method developed in this work yields CFNEs with highly nanostructured surfaces and exposed edge plane sites that may help prevent surface fouling. To evaluate their performance, these CFNEs were tested in human cerebrospinal fluid (CSF) samples, assessing their behavior in this complex biological matrix and their response to the exogenously added neurotransmitters: dopamine, norepinephrine and serotonin.

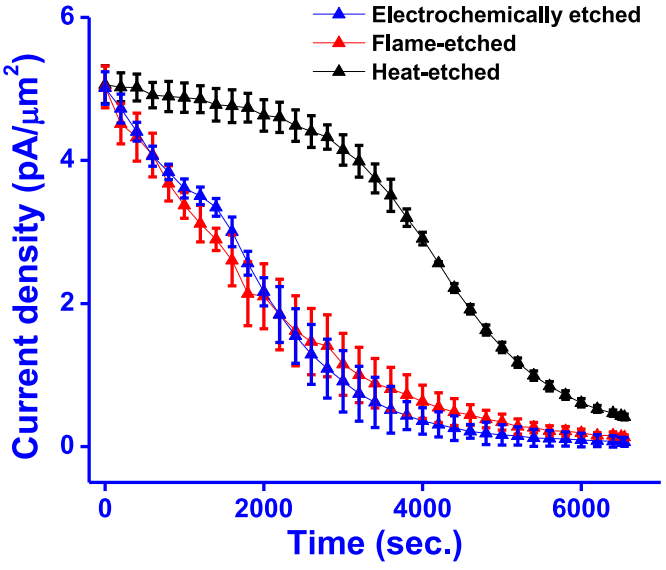

Fig. 9. Amperometric currents recorded during prolonged dopamine oxidation at +0.8 V using electrochemically, flame-, and heat-etched CFNEs in 200 μM dopamine (phosphate buffer, pH 7.4). Data are presented as mean ± S.E.M. ($n = 3$).

Prior to analysis, the CSF solution was diluted 1:1 with 0.1 M phosphate buffer solution (pH 7.4). The heat-etched CFNEs were then placed into the CSF solution, and three consecutive SWV measurements were recorded. The first SWV recording (red line) revealed two oxidation peaks at ~110 mV and ~290 mV (Fig. 10A), likely corresponding to norepinephrine/dopamine and serotonin detection, respectively. These neurotransmitters and their metabolites are commonly present and detectable in CSF [51–55]. In the second SWV recording, both oxidation peak currents decreased while the third consecutive SWV showed only a minor reduction in the oxidation peak currents. The oxidation peak potential at ~290 mV, attributed to serotonin, remained unchanged across consecutive SWVs, whereas the broad peak at ~110 mV became narrower and shifted to ~148 mV, aligning with the expected dopamine peak potential in phosphate buffer.

To test the electrodes response to dopamine in the presence of CSF, the CSF solution was spiked with 1 μM, 5 μM and 10 μM dopamine. The oxidation peak current at ~148 mV increased with the increasing dopamine concentrations (Fig. 10B). At the other side, the oxidation peak at ~290 mV slowly diminished with consecutive SWVs, which could be due to the adsorption of serotonin on the surface of the heat-etched CFNE. This behavior was also observed in the previous voltammetric scan rate experiments with serotonin.

In comparison to heat-etched electrodes, electrochemical and flame-etched electrodes were unable to resolve the separate oxidation peaks for dopamine and serotonin in the CSF sample solution, instead displaying a single broad overlapping peak ranging from 60 mV to 300 mV. In addition, when spiking the CSF sample with 1 μM, 5 μM and 10 μM dopamine, electrochemically and flame-etched electrodes showed a broad oxidation peak at ~175 mV with increasing peak currents as depicted in Fig. 10C and D. In contrast, heat-etched electrodes provided improved resolution of the two oxidation peaks in CSF, corresponding to dopamine and serotonin, and exhibited a sharp oxidation peak in response to spiked dopamine. This suggests that the nanostructured surface of heat-etched electrodes enhances electron transfer kinetics for dopamine oxidation. Therefore, heat-etched CFNEs offer superior properties for reliable electrochemical analysis of neurotransmitters.

3.9. Amperometric detection of norepinephrine in large dense core vesicles of SH-SY5Y cells

To achieve sensitive amperometric recordings of quantal neurotransmission in small cellular spaces such as near synapses of interconnected neurons or inside cells, the conventional carbon fiber microelectrodes need to be miniaturized into nanometric dimensions. Modifying a cylindrical-shaped carbon fiber microelectrode into a cone-shaped geometry with a sharp nano-sized tip enables precise placement at neuronal neurites and also facilitates insertion into the cell cytoplasm for intracellular amperometric measurements of intravesicular neurotransmitter content. Minimizing the electrode length reduces the total electrode surface area and thereby reduces background noise during amperometric measurements. Additionally, intracellular recordings require sharp nanotip electrodes with minimal exposed carbon surface to ensure complete insertion of the electrode into the cell and prevent the detection of molecules released exocytotically [27].

To evaluate the potential of heat-etched CFNEs for single-vesicle

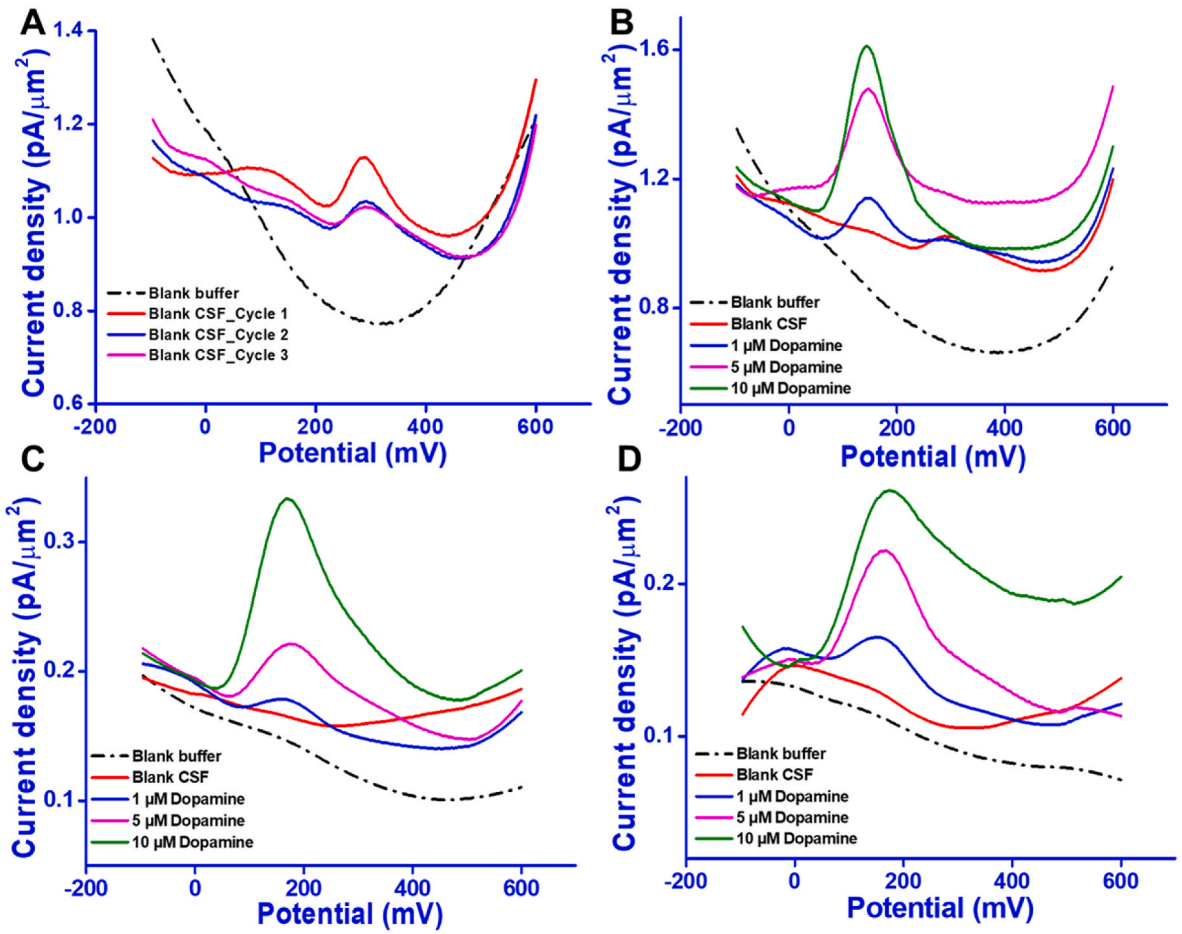

Fig. 10. Testing the sensitivity of heat-etched electrodes for neurotransmitter detection in human CSF. (A) Voltammogram recorded using heat-etched CFNEs in human CSF sample, and (B) after spiking the CSF sample with varying concentrations of dopamine. (C) Voltammograms recorded with electrochemically etched electrodes and (D) flame-etched electrodes in human CSF solution before and after spiking with different concentrations of dopamine. Voltammetry measurements were performed by scanning the potential between −100 and 600 mV against a Ag/AgCl reference electrode. Measurements were performed in triplicate ($n = 3$) for each type of CFNE.

neurotransmitter analysis in single cells, short heat-etched CFNEs were fabricated and applied for intracellular measurements in undifferentiated SH-SY5Y human neuroblastoma cells. SH-SY5Y is an immortalized cancer cell line derived from cells isolated in the 1970s from a neuroblastoma patient's bone marrow biopsy [56,57]. Undifferentiated SH-SY5Y cells have been described as resembling immature catecholaminergic neurons and are widely used for modelling neurodegenerative disorders and neurotoxicity due to their neuronal phenotype and ease of culture [58,59]. These cells have been widely reported to store norepinephrine and neuropeptides in large dense core vesicles (LDCVs) within both the neurites and cell soma [60].

For intracellular recordings, ~10 μm long heat-etched CFNEs were created and inserted into the cell soma using a micromanipulator (Fig. 11A, Fig. S13). Once positioned inside the cell cytoplasm, a constant potential of +800 mV versus an Ag/AgCl reference electrode was applied, enabling the recording of amperometric traces (current versus time) of norepinephrine release. These recordings capture current-versus-time traces as intracellular vesicles rupture upon contact with the electrode surface, triggered by adsorption and the applied electric field (Fig. 11B) [61]. CFNEs showing a stable baseline in bulk cell extracellular media were used for measurements (Fig. 11C). Upon insertion into the cell cytoplasm, these electrodes successfully detected sub-millisecond current spikes with positive amplitude, norepinephrine release from individual vesicles rupturing at the electrode surface (Fig. 11D). Representative data from one successful intracellular recording is shown in Fig. 11, with a second example from another cell provided in Fig. S13.

Fig. 11E presents the averaged amperometric spike ($n = 178$) obtained from intracellular amperometric recording of norepinephrine release from individual vesicles in a single SH-SY5y cell. As illustrated in Fig. 11D, these spikes reflect vesicle rupture at the electrode surface, and the total charge (Q) of each spike can be used to estimate the neurotransmitter content stored in LDCVs. A summary of the analyzed current spike parameters is provided in Fig. 11F. This includes kinetic parameters such as the time duration of the spike (T_{base}), the spike half-width ($T_{1/2}$), the peak rise time (T_{rise}), the peak fall time (T_{fall}), together with the quantitative peak parameters such as the maximum peak amplitude (I_{max}) and the integrated charge Q. Based on the Q value and Faraday's law, the mean number of norepinephrine molecules per LDCV from was estimated to be ~36000. Given that LDCV diameters in SH-SY5Y cells has been reported in a range of 80–130 nm, this corresponds to an estimated intravesicular norepinephrine concentration of 0.05–0.22 M. Similarly, data from a second cell using another heat-etched CFNE ($n = 26$ vesicles, Fig. S14), yielded a higher estimated molecule count of ~157800, corresponding to intravesicular norepinephrine concentrations ranging between 0.23 and 0.98 M. These values are consistent with the range typically reported for LDCVs in PC12 cells and chromaffin cells (0.1–1 M) [62–64], although some studies have reported lower concentrations such as 0.039 M [65] and 0.06–0.07 M [66]. The variability between the two SH-SY5Y cell recordings could be attributed to inherent biological variability between cells or slight variations in electrode properties. A statistically robust analysis would

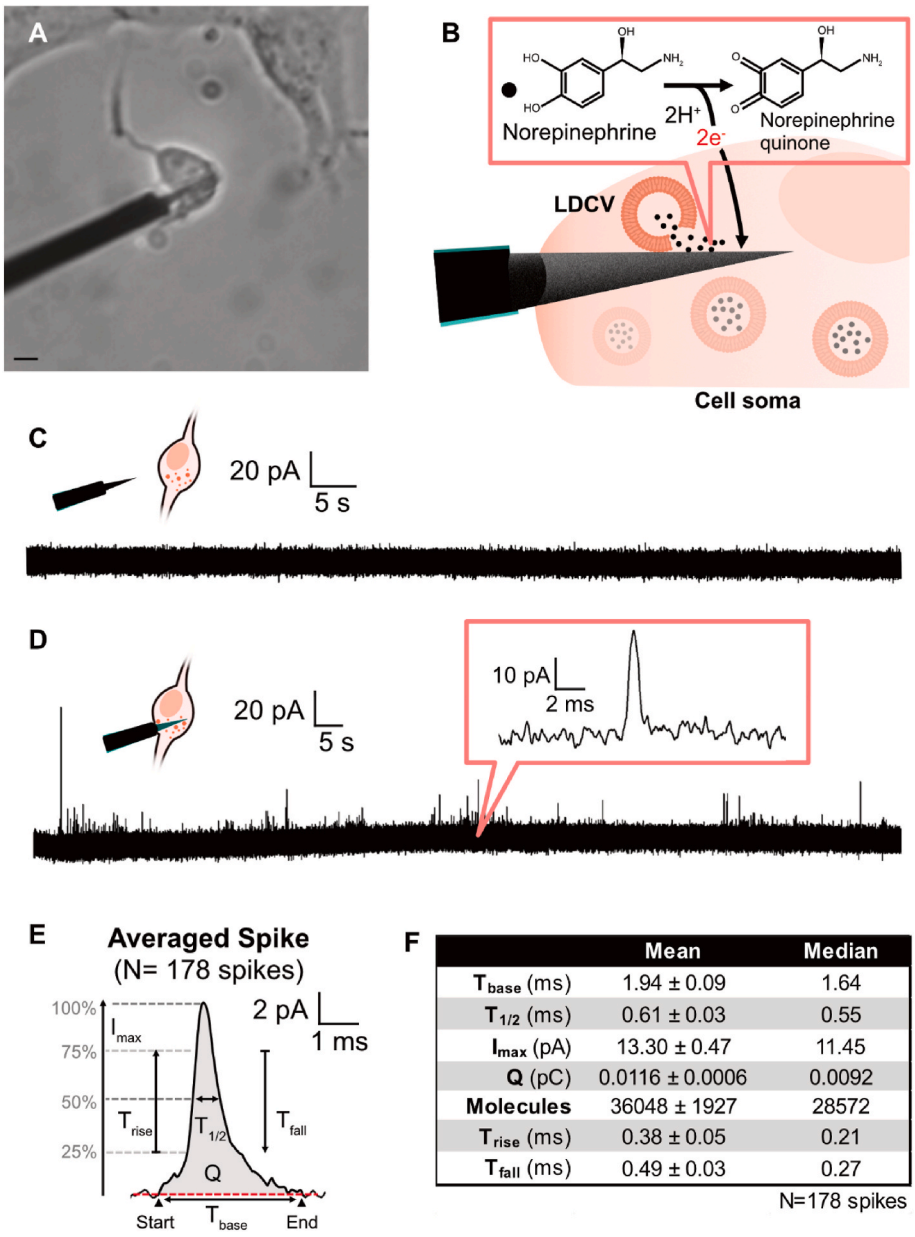

F

	Mean	Median
T_{base} (ms)	1.94 ± 0.09	1.64
$T_{1/2}$ (ms)	0.61 ± 0.03	0.55
I_{max} (pA)	13.30 ± 0.47	11.45
Q (pC)	0.0116 ± 0.0006	0.0092
Molecules	36048 ± 1927	28572
T_{rise} (ms)	0.38 ± 0.05	0.21
T_{fall} (ms)	0.49 ± 0.03	0.27

N=178 spikes

Fig. 11. Intracellular amperometric detection of norepinephrine in SH-SY5Y cells. (A) Brightfield microscopy image of the experimental setup for amperometry showing a 10 μm heat-etched CFNE inserted into the soma of a cell. Scale bar represents 5 μm. (B) Schematic illustration of the detection mechanism of norepinephrine in intracellular vesicles. Inside the cell, norepinephrine released from secretory vesicles is oxidized at the electrode surface, generating a measurable signal. (C) Amperometric recording at +800 mV versus Ag/AgCl before insertion into the cell. (D) Amperometric recording after electrode insertion into the cell. (E) Averaged amperometric spike from 178 events in a single recording and demonstrating spike parameters. I_{max} is the maximum spike amplitude, T_{base} is the spike duration, $T_{1/2}$ is the spike half-width at 50 % of the maximum spike amplitude, T_{rise} is the time to reach to go from 25 % to 75 % of I_{max}, T_{fall} is the time to return from 75 % to 25 % of I_{max} and Q is the integrated charge obtained from the area under the spike. (F) Statistical summary of the spike parameters from 178 intracellular amperometric events presented as the mean ± standard error of the mean (SEM) and median. The number of norepinephrine molecules was estimated using Faraday's law Q = nNF, where Q is the charge, n is the number of electrons participating in the redox reaction (2 for norepinephrine), N is the number of moles of norepinephrine oxidized, and F is the Faraday's constant (96485 C/mol) [74].

require recordings for 15–20 cells to more accurately determine the LDCV quantal content of the SH-SY5Y cells.

Interestingly, the temporal characteristics of amperometric spikes recorded from SH-SY5Y cells using heat-etched CFNEs were shorter than those typically reported for intracellular amperometry for catecholamine vesicles from PC12 and chromaffin cells [67,68]. This is typically seen also during amperometric detection of exocytosis [69] and may be attributed to the inherent differences in LDCV size between the different cell types, with the smaller LDCVs in SH-SY5Y (~80–130 nm) [60], than PC12 cells (~150–240 nm) and chromaffin cells (~340 nm) [70]. These size differences influence both I_{max} and Q, as smaller vesicles contain fewer number of molecules despite having similar intravesicular concentrations [69]. Notably, electrochemical investigations of LDCV content from undifferentiated SH-SY5Y remains unexplored. Only a handful of reports have examined exocytotic catecholamine release from these cells, and none have employed carbon fiber electrodes for detection [69, 71–73]. Reported amperometric exocytotic spike parameters from undifferentiated SH-SY5Y cells vary substantially and, in some cases, suggest intravesicular concentration far exceeding the generally accepted concentration range of 0.1–1 M (Table 1). This discrepancy

Table 1
Comparison of reported intravesicular catecholamine concentrations in undifferentiated SH-SY5Y cells.

Source	Cell type	T1/2 (ms)	Q (pC)	Number of molecules detected	Concentration
This study	SH-SY5Y cell 1 (intracellular amperometry)	0.61	0.012	36000	0.05–0.22 M[a]
This study	SH-SY5Y cell 2 (intracellular amperometry)	0.68	0.051	157800	0.23–0.98 M[a]
Zhao et al. [71]	SH-SY5Y cells (exocytotic recording with ITO micropore electrode)	33	0.654	~2000000	2.89–12.39 M[a]
White et al. [69]	SH-SY5Y cells (exocytotic recording with CMOS chip)	1.63	0.288	~900000	1.30–5.57 M[a]
Shi et al. [72]	SH-SY5Y cells (exocytotic recording with sputtered titanium/platinum)	74	4	~12000000	17.32–74.33 M[a]

[a] The concentration was estimated assuming LDCV diameter of 80–130 nm [60].

may stem from differences in instrumentation or oxidation efficiency across electrode types, warranting further exploration. Finally, although Faraday's law relates the charge detection to the number of molecules undergoing redox reaction in ideal case, real world inefficiencies in electron transfer can influence the accuracy of absolute quantification of the vesicle quantal content.

Despite several attempts to obtain additional recordings, several factors made detection challenging. These include the inherent heterogeneity of undifferentiated SH-SY5Y cells, biological variability in the LDCV number and intravesicular content, and the stochastic nature of vesicle rupture on the electrode surface. Two further recordings resulted in only a single spike each. However, the quantal and temporal properties of these spikes were comparable to those reported, suggesting that they likely represent genuine vesicle rupture events rather than artifacts (Figs. S15 and S16). The primary aim of these experiments was to demonstrate the feasibility of using heat-etched CFNEs for intracellular amperometric detection of vesicular content. A detailed electrochemical characterization of the LDCVs in SH-SY5Y cells lies beyond the scope of this study. How the heat-etched surface modification influence amperometric detection, both during exocytotic catecholamine release and direct LDCV rupture remains to be explored, ideally using chromaffin cells, which are larger, better-characterized and more amenable to such intracellular investigations.

4. Conclusion

The surface morphology of carbon fiber has a great impact on the electrochemical analysis of neurochemicals. This work demonstrates a novel fabrication method for creating short, highly sensitive CFNEs using a time- and temperature-controlled metal heating filament of a glass microcapillary puller. The placement of cylindrical carbon fiber microelectrodes near the filament and applying a heat pulse, results in part of the carbon material being etched away and produces short, cone-shaped, pointy electrodes with tip diameters in the nanometric dimensions. This makes these electrodes well-suited for single-vesicle neurotransmitter analysis at single cells. FE-SEM imaging revealed that the surface of these electrodes features nanocavities and nanodots, which increase the total electrode surface area. Further characterization using Raman spectroscopy indicated that the roughened surface exposes abundant edge plane graphitic sites. Electrochemical analyses comparing CFNEs fabricated using the heat etching method with those produced using conventional electrochemical- and flame-etching methods demonstrated that heat-etched electrodes exhibit higher sensitivity and faster electron transfer kinetics. The electrochemical performance of these electrodes was investigated using cyclic voltammetry and SWV. Compared to conventionally fabricated electrodes, heat-etched electrodes showed higher current density, smaller ΔEp, and lower detection limit for neurotransmitters, indicating that the defect-rich heat-induced surface modifications improve their electrocatalytic properties. Additionally, the heat-etched electrodes exhibited sharper voltammetric peaks in human CSF samples and enabled the simultaneous detection of dopamine and serotonin, unlike conventionally fabricated electrodes. Their highly roughened surface also demonstrated resistance to surface fouling and improved stability during electrochemical analysis. To further validate their practical applicability, short (~10 μm in length) heat-etched CFNEs were used for intracellular recording of single-vesicle neurotransmitter analysis in single SH-SY5Y cells. These electrodes successfully detected the sub-millisecond release of norepinephrine from single vesicles upon contact with the electrode surface. Therefore, the method of producing sharp CFNEs using heat-etching offers a simple method that provides a high fabrication success rate and does not cause damage to the glass seal, which is a common challenge in conventional fabrication techniques (Fig. S17). Moreover, they provide enhanced sensitivity due to the heat-induced surface modifications. Altogether, heat-etching presents a reliable alternative to traditional methods for fabricating sharp CFNEs, which creates electrodes with improved performance for neurotransmitter detection and intracellular electrochemical analysis.

CRediT authorship contribution statement

Pankaj Gupta: Writing – review & editing, Writing – original draft, Validation, Software, Methodology, Investigation, Formal analysis, Data curation, Conceptualization. **Ajay Pradhan:** Writing – review & editing, Writing – original draft, Validation, Software, Methodology, Investigation, Formal analysis, Data curation. **Vandna K. Gupta:** Formal analysis, Data curation. **Hanna Karlsson-Fernberg:** Formal analysis. **Yuanmo Wang:** Writing – review & editing, Methodology, Conceptualization. **Jörg Hanrieder:** Resources. **Henrik Zetterberg:** Resources, Funding acquisition. **Ann-Sofie Cans:** Writing – review & editing, Supervision, Resources, Methodology, Funding acquisition, Conceptualization.

Funding

This work was funded by The Swedish Research Council (VR-2020-04920), the Carl Trygger Foundation, the Chalmers Genie Initiative, and the Chalmers Nano Area of Advance. HZ is a Wallenberg Scholar and a Distinguished Professor at the Swedish Research Council supported by grants from the Swedish Research Council (#2023-00356,#2022-01018 and #2019–02397), the European Union's Horizon Europe research and innovation program under grant agreement No 101053962, and Swedish State Support for Clinical Research (#ALFGBG-71320).

Declaration of competing interest

The authors declare that they have no known competing financial interests or personal relationships that could have appeared to influence the work reported in this paper.

Acknowledgments

We thank the Anna Martinelli lab at the Department of Chemistry and Chemical Engineering, Chalmers University of Technology for allowing us to use the Raman microscope in your lab. We also thank Chalmers Materials Analysis Laboratory (CMAL) for the instrumentations and technical support for FE-SEM and EDX.

Appendix A. Supplementary data

Supplementary data to this article can be found online at https://doi.org/10.1016/j.carbon.2025.120612.

References

[1] R.M. Wightman, Voltammetry with microscopic electrodes in new domains, Science 240 (1988) 415–420, https://doi.org/10.1126/science.240.4851.415.
[2] K.P. Troyer, M.L.A. Heien, B.J. Venton, R.M. Wightman, Neurochemistry and electroanalytical probes, Curr. Opin. Chem. Biol. 6 (2002) 696–703, https://doi.org/10.1016/S1367-5931(02)00374-5.
[3] J.M. Kita, R.M. Wightman, Microelectrodes for studying neurobiology, Curr. Opin. Chem. Biol. 12 (2008) 491–496, https://doi.org/10.1016/j.cbpa.2008.06.035.
[4] J.D. Keighron, Y. Wang, A.-S. Cans, Electrochemistry of single-vesicle events, Annu. Rev. Anal. Chem. 13 (2020) 159–181, https://doi.org/10.1146/annurev-anchem-061417-010032.
[5] P.S. Cahill, Q.D. Walker, J.M. Finnegan, G.E. Mickelson, E.R. Travis, R. M. Wightman, Microelectrodes for the measurement of catecholamines in biological systems, Anal. Chem. 68 (1996) 3180–3186, https://doi.org/10.1021/ac960347d.
[6] Z. Shao, Y. Chang, B.J. Venton, Carbon microelectrodes with customized shapes for neurotransmitter detection: a review, Anal. Chim. Acta 1223 (2022) 340165, https://doi.org/10.1016/j.aca.2022.340165.
[7] M.L. Huffman, B.J. Venton, Carbon-fiber microelectrodes for in vivo applications, Analyst 134 (2009) 18–24, https://doi.org/10.1039/B807563H.
[8] D.J. Leszczyszyn, J.A. Jankowski, O.H. Viveros, E.J. Diliberto, J.A. Near, R. M. Wightman, Nicotinic receptor-mediated catecholamine secretion from individual chromaffin cells. Chemical evidence for exocytosis, J. Biol. Chem. 265 (1990) 14736–14737, https://doi.org/10.1016/S0021-9258(18)77173-1.
[9] Y. Fan, C. Han, B. Zhang, Recent advances in the development and application of nanoelectrodes, Analyst 141 (2016) 5474–5487, https://doi.org/10.1039/C6AN01285J.
[10] S. Marinesco, Micro- and nano-electrodes for neurotransmitter monitoring, Curr. Opin. Electrochem. 29 (2021) 100746, https://doi.org/10.1016/j.coelec.2021.100746.
[11] J.L. Ponchon, R. Cespuglio, F. Gonon, M. Jouvet, J.F. Pujol, Normal pulse polarography with carbon fiber electrodes for in vitro and in vivo determination of catecholamines, Anal. Chem. 51 (1979) 1483–1486, https://doi.org/10.1021/ac50045a030.
[12] A. Hatamie, X. He, X.-W. Zhang, P.E. Oomen, A.G. Ewing, Advances in nano/microscale electrochemical sensors and biosensors for analysis of single vesicles, a key nanoscale organelle in cellular communication, Biosens. Bioelectron. 220 (2023) 114899, https://doi.org/10.1016/j.bios.2022.114899.
[13] B.E.K. Swamy, B.J. Venton, Carbon nanotube-modified microelectrodes for simultaneous detection of dopamine and serotonin in vivo, Analyst 132 (2007) 876, https://doi.org/10.1039/b705552h.
[14] A.J. Syeed, Y. Li, B.J. Ostertag, J.W. Brown, A.E. Ross, Nanostructured carbon-fiber surfaces for improved neurochemical detection, Faraday Discuss 233 (2022) 336–353, https://doi.org/10.1039/D1FD00049G.
[15] P. Takmakov, M.K. Zachek, R.B. Keithley, P.L. Walsh, C. Donley, G.S. McCarty, R. M. Wightman, Carbon microelectrodes with a renewable surface, Anal. Chem. 82 (2010) 2020–2028, https://doi.org/10.1021/ac902753x.
[16] M. Zhang, K. Liu, L. Xiang, Y. Lin, L. Su, L. Mao, Carbon nanotube-modified carbon fiber microelectrodes for in vivo voltammetric measurement of ascorbic acid in rat brain, Anal. Chem. 79 (2007) 6559–6565, https://doi.org/10.1021/ac0705871.
[17] L. Xiang, P. Yu, J. Hao, M. Zhang, L. Zhu, L. Dai, L. Mao, Vertically aligned carbon nanotube-sheathed carbon fibers as pristine microelectrodes for selective monitoring of ascorbate in vivo, Anal. Chem. 86 (2014) 3909–3914, https://doi.org/10.1021/ac404232h.
[18] M.E. Weese, R.A. Krevh, Y. Li, N.T. Alvarez, A.E. Ross, Defect sites modulate fouling resistance on carbon-nanotube Fiber electrodes, ACS Sens. 4 (2019) 1001–1007, https://doi.org/10.1021/acssensors.9b00161.
[19] Q. Cao, P. Puthongkham, B.J. Venton, Review: new insights into optimizing chemical and 3D surface structures of carbon electrodes for neurotransmitter detection, Anal. Methods 11 (2019) 247–261, https://doi.org/10.1039/c8ay02472c.
[20] Q. Cao, Z. Shao, D. Hensley, B.J. Venton, Carbon nanospike coated nanoelectrodes for measurements of neurotransmitters, Faraday Discuss 233 (2022) 303–314, https://doi.org/10.1039/D1FD00053E.
[21] Q. Cao, D.K. Hensley, N.V. Lavrik, B.J. Venton, Carbon nanospikes have better electrochemical properties than carbon nanotubes due to greater surface roughness and defect sites, Carbon N. Y. 155 (2019) 250–257, https://doi.org/10.1016/j.carbon.2019.08.064.
[22] M. Armstrong-James, K. Fox, J. Millar, A method for etching the tips of carbon fibre microelectrodes, J. Neurosci. Methods 2 (1980) 431–432, https://doi.org/10.1016/0165-0270(80)90009-6.
[23] A. Meulemans, B. Poulain, G. Baux, L. Tauc, D. Henzel, Micro carbon electrode for intracellular voltammetry, Anal. Chem. 58 (1986) 2088–2091, https://doi.org/10.1021/ac00122a035.
[24] K.T. Kawagoe, J.A. Jankowski, R.M. Wightman, Etched carbon-fiber electrodes as amperometric detectors of catecholamine secretion from isolated biological cells, Anal. Chem. 63 (1991) 1589–1594, https://doi.org/10.1021/ac00015a017.
[25] E.E.-D.M. El-Giar, D.O. Wipf, Preparation of tip-protected poly(oxyphenylene) coated carbon-fiber ultramicroelectrodes, Electroanalysis 18 (2006) 2281–2289, https://doi.org/10.1002/elan.200603637.
[26] H. Khani, D.O. Wipf, Fabrication of tip-protected polymer-coated carbon-fiber ultramicroelectrodes and pH ultramicroelectrodes, J. Electrochem. Soc. 166 (2019) B673–B679, https://doi.org/10.1149/2.0941908jes.
[27] J.G. Roberts, E.C. Mitchell, L.E. Dunaway, G.S. McCarty, L.A. Sombers, Carbon-Fiber nanoelectrodes for real-time discrimination of vesicle cargo in the native cellular environment, ACS Nano 14 (2020) 2917–2926, https://doi.org/10.1021/acsnano.9b07318.
[28] T.G. Strein, A.G. Ewing, Characterization of submicron-sized carbon electrodes insulated with a phenol-allylphenol copolymer, Anal. Chem. 64 (1992) 1368–1373, https://doi.org/10.1021/ac00037a012.
[29] A.M. Strand, B.J. Venton, Flame etching enhances the sensitivity of carbon-fiber microelectrodes, Anal. Chem. 80 (2008) 3708–3715, https://doi.org/10.1021/ac8001275.
[30] X. Li, S. Majdi, J. Dunevall, H. Fathali, A.G. Ewing, Quantitative measurement of transmitters in individual vesicles in the cytoplasm of single cells with nanotip electrodes, Angew. Chemie - Int. Ed. 54 (2015) 11978–11982, https://doi.org/10.1002/anie.201504839.
[31] H. Fathali, J. Dunevall, S. Majdi, A.-S. Cans, Extracellular osmotic stress reduces the vesicle size while keeping a constant neurotransmitter concentration, ACS Chem. Neurosci. 8 (2017) 368–375, https://doi.org/10.1021/acschemneuro.6b00350.
[32] A.G. Zestos, C. Yang, C.B. Jacobs, D. Hensley, B.J. Venton, Carbon nanospikes grown on metal wires as microelectrode sensors for dopamine, Analyst 140 (2015) 7283–7292, https://doi.org/10.1039/C5AN01467K.
[33] H.R. Rees, S.E. Anderson, E. Privman, H.H. Bau, B.J. Venton, Carbon nanopipette electrodes for dopamine detection in *Drosophila*, Anal. Chem. 87 (2015) 3849–3855, https://doi.org/10.1021/ac504596y.
[34] Q. Cao, M. Shin, N.V. Lavrik, B.J. Venton, 3D-Printed carbon nanoelectrodes for in vivo neurotransmitter sensing, Nano Lett. 20 (2020) 6831–6836, https://doi.org/10.1021/acs.nanolett.0c02844.
[35] G.D. Christian, W.C. Purdy, The residual current in orthophosphate medium, J. Electroanal. Chem. 3 (1962) 363–367, https://doi.org/10.1016/0022-0728(62)80012-6.
[36] Y. Wang, H. Fathali, D. Mishra, T. Olsson, J.D. Keighron, K.P. Skibicka, A.-S. Cans, Counting the number of glutamate molecules in single synaptic vesicles, J. Am. Chem. Soc. 141 (2019) 17507–17511, https://doi.org/10.1021/jacs.9b09414.
[37] E.V. Mosharov, D. Sulzer, Analysis of exocytotic events recorded by amperometry, Nat. Methods 2 (2005) 651–658, https://doi.org/10.1038/nmeth782.
[38] P. Gupta, R.A. Lazenby, C.E. Rahm, W.R. Heineman, E. Buschbeck, R.J. White, N. T. Alvarez, Electrochemistry of controlled diameter carbon nanotube fibers at the cross section and sidewall, ACS Appl. Energy Mater. 2 (2019) 8757–8766, https://doi.org/10.1021/acsaem.9b01723.
[39] K.-W. Kim, J.-S. Jeong, K.-H. An, B.-J. Kim, A study on the microstructural changes and mechanical behaviors of carbon fibers induced by optimized electrochemical etching, Compos. Part B Eng. 165 (2019) 764–771, https://doi.org/10.1016/j.compositesb.2019.02.055.
[40] A. Sadezky, H. Muckenhuber, H. Grothe, R. Niessner, U. Pöschl, Raman microspectroscopy of soot and related carbonaceous materials: spectral analysis and structural information, Carbon N. Y. 43 (2005) 1731–1742, https://doi.org/10.1016/j.carbon.2005.02.018.
[41] J. Wu, Understanding the electric double-layer structure, capacitance, and charging dynamics, Chem. Rev. 122 (2022) 10821–10859, https://doi.org/10.1021/acs.chemrev.2c00097.
[42] J. Wei, Y. Li, D. Dai, F. Zhang, H. Zou, X. Yang, Y. Ji, B. Li, X. Wei, Surface roughness: a crucial factor to robust electric double layer capacitors, ACS Appl. Mater. Interfaces 12 (2020) 5786–5792, https://doi.org/10.1021/acsami.9b18799.
[43] S. Torabi, M. Cherry, E.A. Duijnstee, V.M. Le Corre, L. Qiu, J.C. Hummelen, G. Palasantzas, L.J.A. Koster, Rough electrode creates excess capacitance in thin-film capacitors, ACS Appl. Mater. Interfaces 9 (2017) 27290–27297, https://doi.org/10.1021/acsami.7b06451.
[44] N. Kurapati, P. Pathirathna, R. Chen, S. Amemiya, Voltammetric measurement of adsorption isotherm for ferrocene derivatives on highly oriented pyrolytic graphite, Anal. Chem. 90 (2018) 13632–13639, https://doi.org/10.1021/acs.analchem.8b03883.
[45] J.C. Zuaznabar-Gardona, A. Fragoso, Electrochemical characterisation of the adsorption of ferrocenemethanol on carbon nano-onion modified electrodes, J. Electroanal. Chem. 871 (2020), https://doi.org/10.1016/j.jelechem.2020.114314.
[46] K.J. Aoki, J. Chen, Y. Liu, B. Jia, Peak potential shift of fast cyclic voltammograms owing to capacitance of redox reactions, J. Electroanal. Chem. 856 (2020) 113609, https://doi.org/10.1016/j.jelechem.2019.113609.
[47] K. Aoki, K. Honda, K. Tokuda, H. Matsuda, Voltammetry at microcylinder electrodes, J. Electroanal. Chem. Interfacial Electrochem. 182 (1985) 267–279, https://doi.org/10.1016/0368-1874(85)87005-2.
[48] D. Zhao, D. Siebold, N.T. Alvarez, V.N. Shanov, W.R. Heineman, Carbon nanotube thread electrochemical cell: detection of heavy metals, Anal. Chem. 89 (2017) 9654–9663, https://doi.org/10.1021/acs.analchem.6b04724.
[49] W. Harreither, R. Trouillon, P. Poulin, W. Neri, A.G. Ewing, G. Safina, Carbon nanotube fiber microelectrodes show a higher resistance to dopamine fouling, Anal. Chem. 85 (2013) 7447–7453, https://doi.org/10.1021/ac401399s.

[50] A.C. Schmidt, X. Wang, Y. Zhu, L.A. Sombers, Carbon nanotube yarn electrodes for enhanced detection of neurotransmitter dynamics in live brain tissue, ACS Nano 7 (2013) 7864–7873, https://doi.org/10.1021/nn402857u.
[51] T. Seppala, M. Scheinin, A. Capone, M. Linnoila, Liquid chromatographic assay for CSF catecholamines using electrochemical detection, Acta Pharmacol. Toxicol. 55 (1984) 81–87, https://doi.org/10.1111/j.1600-0773.1984.tb01966.x.
[52] J. Wagner, P. Vitali, M.G. Palfreyman, M. Zraika, S. Huot, Simultaneous determination of 3,4-Dihydroxyphenylalanine, 5-Hydroxytryptophan, dopamine, 4-Hydroxy-3-Methoxyphenylalanine, norepinephrine, 3,4-Dihydroxyphenylacetic acid, homovanillic acid, serotonin, and 5-Hydroxyindoleacetic acid in rat cerebrospinal fluid and brain by high-performance liquid chromatography with electrochemical detection, J. Neurochem. 38 (1982) 1241–1254, https://doi.org/10.1111/j.1471-4159.1982.tb07897.x.
[53] M. Senel, E. Dervisevic, S. Alhassen, M. Dervisevic, A. Alachkar, V.J. Cadarso, N. H. Voelcker, Microfluidic electrochemical sensor for cerebrospinal fluid and blood dopamine detection in a mouse model of parkinson's disease, Anal. Chem. 92 (2020) 12347–12355, https://doi.org/10.1021/acs.analchem.0c02032.
[54] M. Batllori, M. Molero-Luis, A. Ormazabal, M. Casado, C. Sierra, A. García-Cazorla, M. Kurian, S. Pope, S.J. Heales, R. Artuch, Analysis of human cerebrospinal fluid monoamines and their cofactors by HPLC, Nat. Protoc. 12 (2017) 2359–2366, https://doi.org/10.1038/nprot.2017.103.
[55] T. Suominen, P. Uutela, R.A. Ketola, J. Bergquist, L. Hillered, M. Finel, H. Zhang, A. Laakso, R. Kostiainen, Determination of serotonin and dopamine metabolites in human brain microdialysis and cerebrospinal fluid samples by UPLC-MS/MS: discovery of intact glucuronide and sulfate conjugates, PLoS One 8 (2013) e68007, https://doi.org/10.1371/journal.pone.0068007.
[56] J.L. Biedler, S. Roffler-Tarlov, M. Schachner, L.S. Freedman, Multiple neurotransmitter synthesis by human neuroblastoma cell lines and clones, Cancer Res. 38 (1978) 3751–3757. http://cancerres.aacrjournals.org/content/38/11_Part_1/3751http://cancerres.aacrjournals.org/content/38/11_Part_1/3751#related-urls.
[57] J.L. Biedler, L. Helson, B.A. Spengler, Morphology and growth, tumorigenicity, and cytogenetics of human neuroblastoma cells in continuous Culture1, Cancer Res. 33 (1973) 2643–2652.
[58] J. Kovalevich, D. Langford, Considerations for the use of SH-SY5Y neuroblastoma cells in neurobiology, Methods Mol. Biol. (2013) 9–21, https://doi.org/10.1007/978-1-62703-640-5_2.
[59] H. Xicoy, B. Wieringa, G.J.M. Martens, The SH-SY5Y cell line in Parkinson's disease research: a systematic review, Mol. Neurodegener. 12 (2017) 10, https://doi.org/10.1186/s13024-017-0149-0.
[60] X.M. Ou, P.M. Partoens, J.M. Wang, J.H. Walker, K. Danks, P.F. Vaughan, W.P. De Potter, The storage of noradrenaline, neuropeptide Y and chromogranins in and stoichiometric release from large dense cored vesicles of the undifferentiated human neuroblastoma cell line SH-SY5Y, Int. J. Mol. Med. 1 (1998) 105–112, https://doi.org/10.3892/ijmm.1.1.105.
[61] J. Dunevall, S. Majdi, A. Larsson, A. Ewing, Vesicle impact electrochemical cytometry compared to amperometric exocytosis measurements, Curr. Opin. Electrochem. 5 (2017) 85–91, https://doi.org/10.1016/j.coelec.2017.07.005.
[62] T.L. Colliver, S.J. Pyott, M. Achalabun, A.G. Ewing, VMAT-mediated changes in quantal size and vesicular volume, J. Neurosci. 20 (2000) 5276–5282, https://doi.org/10.1523/JNEUROSCI.20-14-05276.2000.
[63] L. Ren, A. Oleinick, I. Svir, C. Amatore, A.G. Ewing, Amperometric measurements and dynamic models reveal a mechanism for how zinc alters neurotransmitter release, Angew. Chemie Int. Ed. 59 (2020) 3083–3087, https://doi.org/10.1002/anie.201913184.
[64] X.-W. Zhang, A. Hatamie, A.G. Ewing, Simultaneous quantification of vesicle size and catecholamine content by resistive pulses in nanopores and vesicle impact electrochemical cytometry, J. Am. Chem. Soc. 142 (2020) 4093–4097, https://doi.org/10.1021/jacs.9b13221.
[65] S. Rabasco, T.D.K. Nguyen, C. Gu, M.E. Kurczy, N.T.N. Phan, A.G. Ewing, Localization and absolute quantification of dopamine in discrete intravesicular compartments using NanoSIMS imaging, Int. J. Mol. Sci. 23 (2021) 160, https://doi.org/10.3390/ijms23010160.
[66] X. Li, J. Dunevall, A.G. Ewing, Electrochemical quantification of transmitter concentration in single nanoscale vesicles isolated from PC12 cells, Faraday Discuss 210 (2018) 353–364, https://doi.org/10.1039/C8FD00020D.
[67] S. Majdi, A. Larsson, N. Najafinobar, R. Borges, A.G. Ewing, Extracellular ATP regulates the vesicular pore opening in chromaffin cells and increases the fraction released during individual exocytosis events, ACS Chem. Neurosci. 10 (2019) 2459–2466, https://doi.org/10.1021/acschemneuro.8b00722.
[68] Y. Wang, C. Gu, A.G. Ewing, A multimodal electrochemical approach to measure the effect of zinc on vesicular content and exocytosis in a single cell model of ischemia, QRB Discov. 2 (2021) e12, https://doi.org/10.1017/qrd.2021.10.
[69] K.A. White, G. Mulberry, J. Smith, M. Lindau, B.A. Minch, K. Sugaya, B.N. Kim, Single-cell recording of vesicle release from human neuroblastoma cells using 1024-ch monolithic CMOS bioelectronics, IEEE Trans. Biomed. Circuits Syst. 12 (2018) 1345–1355, https://doi.org/10.1109/TBCAS.2018.2861220.
[70] R.H.S. Westerink, A.G. Ewing, The PC12 cell as model for neurosecretion, Acta Physiol. 192 (2008) 273–285, https://doi.org/10.1111/j.1748-1716.2007.01805.x.
[71] H. Zhao, L. Li, H.-J. Fan, F. Wang, L.-M. Jiang, P.-G. He, Y.-Z. Fang, Exocytosis of SH-SY5Y single cell with different shapes cultured on ITO micro-pore electrode, Mol. Cell. Biochem. 363 (2012) 309–313, https://doi.org/10.1007/s11010-011-1183-9.
[72] B.-X. Shi, Y. Wang, T.-L. Lam, W.-H. Huang, K. Zhang, Y.-C. Leung, H.L.W. Chan, Release monitoring of single cells on a microfluidic device coupled with fluorescence microscopy and electrochemistry, Biomicrofluidics 4 (2010), https://doi.org/10.1063/1.3491470.
[73] H. Zhao, F. Zhang, L. Li, P. He, Y. Fang, Exocytosis determination of SH-SY5Y single cell stimulated by different stimulants on indium tin oxide (ITO) micro-pore electrode, Biocell 37 (2013) 77–83, https://doi.org/10.32604/biocell.2013.37.077.
[74] E.R. Travis, R.M. Wightman, SPATIO-TEMPORAL resolution of exocytosis from individual cells, Annu. Rev. Biophys. Biomol. Struct. 27 (1998) 77–103, https://doi.org/10.1146/annurev.biophys.27.1.77.